STATE OF CALIFORNIA • DEPARTMENT OF TRANSPORTATION

TECHNICAL REPORT DOCUMENTATION PAGE

TR0003 (REV 10/98)

ADA Notice

For individuals with sensory disabilities, this document is available in alternate formats. For information call (916) 654-6410 or TDD (916) 654-3880 or write Records and Forms Management, 1120 N Street, MS-89, Sacramento, CA 95814.

1. REPORT NUMBER	2. GOVERNMENT ASSOCIATION NUMBER	3. RECIPIENT'S CATALOG NUMBER
CA11-1228		

4. TITLE AND SUBTITLE

DSRC Standards testing: 5MHz Band-plan Analysis, Clustered System Architecture and Communication in Emergency Scenarios

5. REPORT DATE

December 12, 2011

6. PERFORMING ORGANIZATION CODE

7. AUTHOR

Danijela Cabric, Jared Dulmage, Wesam Gabran, Lucas Araki

8. PERFORMING ORGANIZATION REPORT NO.

9. PERFORMING ORGANIZATION NAME AND ADDRESS

UCLA
11000 Kinross Avenue, Suite 102
Los Angeles, CA 90095-1406

10. WORK UNIT NUMBER

11. CONTRACT OR GRANT NUMBER

65A0292

12. SPONSORING AGENCY AND ADDRESS

California Department of Transportation
Division of Research and Innovation, MS-83
1227 O Street
Sacramento CA 95814

13. TYPE OF REPORT AND PERIOD COVERED

Final

14. SPONSORING AGENCY CODE

15. SUPPLEMENTARY NOTES

16. ABSTRACT

Researchers performed a system level technical study of physical layer and network layer performance of vehicular communication in a specially licensed Dedicated Short Range Communication (DSRC) 5.9 GHz frequency band. Physical layer analysis provides complete understanding of OFDM based 802.11p performance parameterized by packet length, modulation type, vehicular channels and signal-to-noise ratio. Network level analysis of co-channel and adjacent channel interference, using detailed NS-2 simulation model, takes into account impact of collisions and access protocol on QoS and packet delivery ratios. Simulations considered large set of traffic scenarios and characterized the required power levels to achieve given transmission range. Lastly, the feasibility study of practical cooperative localization algorithms for robust prediction and avoidance of accidents is presented.

17. KEY WORDS	18. DISTRIBUTION STATEMENT
Wireless Access in Vehicular Environments (WAVE), Dedicated Short Range Communications (DSRC), Physical layer communication, OFDM, wireless vehicular networks, Simulation platforms, 802.11p, 5.9 GHz Band, Localization, Global Positioning System (GPS)	No restrictions. This document is available to the public through the National Technical Information Service, Springfield, VA 22161

19. SECURITY CLASSIFICATION *(of this report)*	20. NUMBER OF PAGES	21. COST OF REPORT CHARGED
Unclassified	53	

Noisy GPS based initial position of all cars

Noisy RSS data from all vehicle pairs

All vehicles positions

Velocity sensor data of all cars

State Prediction (x-y coords of all cars) using a simple noisy Dynamics model

Update State using RSS data

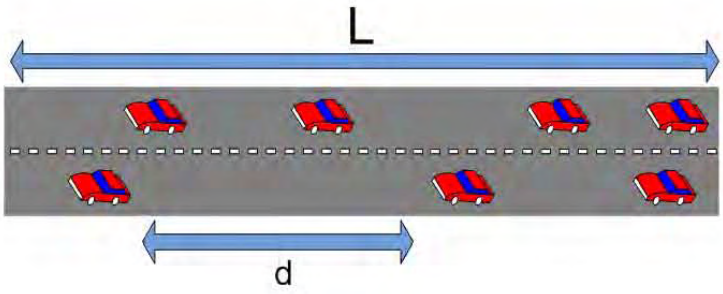

DSRC Standards testing: 5MHz band-plan analysis, clustered system architecture and communication in emergency scenarios

Final Report for Contract 65A0292 with
California Department of Transportation
Division of Research and Innovation
Office of Technology Applications

Danijela Cabric, Jared Dulmage, Wesam Gabran, Lucas Araki
Cognitive Reconfigurable Embedded Systems Lab
Electrical Engineering Department
University of California, Los Angeles

Federal Report Number CA11-1228
Caltrans Contract # 65A0292, Project ID 0000000603
December 12, 2011

Acknowledgments

This is the final report of the project "(Continuation of T.O. 6214) ITS Band Roadside to Vehicle Communications in a Highway Setting", which was sponsored by the Department of Transportation of California (Caltrans) under Task Orders 6214. We would like to acknowledge the Project Manager for Caltrans, Gloria Gwynne, Senior Transportation Electrical Engineer, Office of Technology Applications, and Ramez Gerges, Chief, Office of Communication Systems, Caltrans Department of Research and Innovation, for their technical insights and tremendous organizational support.

Disclaimer

The contents of this report reflect the views of the authors who are responsible for the facts and the accuracy of the data presented herein. The contents do not necessarily reflect the official views or policies of the State of California or the Federal Highway Administration. This report does not constitute a standard, specification or regulation.

The State of California does not endorse products or manufacturers. Trade and manufacturers' names appear in this report only because they are considered essential to the object of the document.

Executive Summary

This report presents a system level technical study of physical layer performance and network layer analysis of vehicular communication in a specially licensed Dedicated Short Range Communication (DSRC) 5.9 GHz frequency band.

Section I presents a comprehensive set of simulation tests that characterize the packet error rate performance of 802.11p compliant physical layer link as a function of several system and channel parameters including packet length, modulation scheme, SNR, fading channel and receiver functions including time/frequency offset tracking and channel tracking. By considering specific applications and their requirements, we evaluated how large packets should be used in order to minimize the total number of transmitted packets, and thus transmission time or application latency.

In Section II we extended the analysis of packet delivery rates in different traffic scenarios using network layer simulation tool NS-2. By considering several traffic densities (characterized by average vehicle separation of 5m, 10m, and 30m) we investigated the impact of collisions on packet reception and characterized the probability of successful transmission (i.e. outage) as function of transmission range for different transmitter power levels.

Section III analyzes the effect of adjacent channel interference between safety, control and service channels based on the current DSRC frequency plan through mathematical modeling and NS2 simulations. Results show acceptable levels of SINR degradation in all cases except when vehicles are equipped with 2 radios that simultaneously transmit on the safety channel and its neighboring channel.

In Section IV we explored cooperative localization algorithms that would enable robust prediction and avoidance of accidents among many other safety applications. The main challenge in this thrust was the requirement on localization accuracy in the order of 0.5m. We present two different approaches for accurate localization of vehicles. The first approach relies on estimating the relative distances between vehicles by analyzing the strength of the communication signals between them. The second approach relies on Global Positioning System (GPS) data.

Table of Contents

List of Figures

List of Tables

II. Physical Layer Performance Analysis

A. Introduction

Intelligent Transportation Systems (ITS) aim to improve both the safety and efficiency of the country's roadways by improving the situational awareness (SA) of each vehicle in its local area and that of transportation authorities over their administrative region. This will be enabled by Dedicated Short Range Communications (DSRC), a set of wireless communication systems that link vehicles to each other (V2V) and roadside infrastructure (V2I). DSRC encompasses a number of wireless technologies, however the most versatile, detailed in IEEE 802.11p draft standard 24, is envisioned as the single communications conduit over which most, if not all, applications will operate.

Inherent to SA is information on the location and trajectories of vehicles on the road. Each vehicle periodically broadcasts this information to vehicles in its area and, possibly, to roadside units which may relay the information to traffic monitoring centers. Based on the location, speed, heading, and other dynamics of nearby vehicles, a driver could be advised of changes in traffic conditions beyond their sight and even warned of an impending collisions.
Because safety-of-life is at stake, it is imperative that the vehicular network operate even under high load and unfavorable environments for communication. In particular, when traffic is dense, the capacity of the network, i.e. the number of messages that can be successfully disseminated, must be sufficient to service the high message volume with a high success rate. There are a number of factors that affect network capacity, primarily the wireless radio, the wireless propagation environment, and the multiple access control (MAC).
This report is based on the research detailed in 24.

B. The wireless radio

The *physical layer (PHY)* refers to the radio hardware that generates signals sent by the transmitter and decodes signals at the receiver. The IEEE 802.11p draft standard specifies Orthogonal Frequency Division Multiplexing (OFDM) for its signaling technology. A comprehensive description of OFDM and common hardware signal processing algorithms are beyond the scope of this report, however there are numerous sources available for reference (e.g. 24 and 24). In brief, OFDM enables efficient, high data rate communications with low cost radio hardware. It is a proven technology for both wired (DSL) and wireless (IEEE 802.11a/g WiFi) systems and has been chosen for next generation cellular communications (WiMAX and Long Term Evolution or LTE) as well.

C. The wireless channel

When two radios communicate, the transmitted signal undergoes a number of changes on its way to the receiver. First, the signal is attenuated, or becomes weaker, due to the distance it has traveled. Second, the signal is distorted being reflected off and absorbed by obstacles in the environment. The totality of the affects of distance and the environment on the signal is termed

the *wireless channel*. It is often shortened to simply the *channel*. A system may experience many different channels, offering harsh or benign conditions for propagation, depending on the environment and the placement of the transmit and receive antennas. Communications systems are often designed to work adequately in an average or typical environment. For vehicular networks it is important that the system operate well even in harsh environments.

Signal attenuation is often called *fading*, evoking the sound of the whistle of a departing train. Large-scale fading refers to that due to distance. In contrast, small-scale fading refers to the somewhat random attenuation experienced by signals over distances on the order of the signal wavelength. For IEEE 802.11p this can be a meter or less. Small-scale fading is the affect often encountered while talking on a cellular phone. In one place, signal strength is strong and the voice over the phone is clear, whereas a couple steps away the signal strength is weak, the voice quality degrades, and the call may even be dropped.

Small-scale fading results from the combination of signals at the receiver which have reflected off obstacles in the environment. Different signals, having taken different paths to the receiver, may combine constructively or destructively depending on the precise geometry of the transmitter, receiver, and obstacles. If all of these objects are stationary the channel is called *static* and the signal strength at a fixed location will not change. However, if anything in the environment is moving, the channel is called *time-varying* or *dynamic* and the signal strength will vary with time. The rate at which a channel varies depends on the speed of the objects within the environment.

The conventional measure of the time-variation of the channel is the *coherence time*. Consider the aforementioned cellular phone scenario. The received the signal was strong in one location and weak say d meters away. If you, the receiver, were traveling at some speed v, the time that it would take to move from a strong to weak fade (or vice versa) would be $T_C=d/v$, the coherence time. This simplified definition conveys the intuitive relationship that the channel changes in less time as ones speed increases. Coherence time is rigorously defined as a function of the statistical auto-correlation of the channel. While less precise, the simplified definition is sufficient for the explanations in this report.

D. Methodology

Mathematical models quantitatively describe the relationship between system variables or parameters and the behavior of the system. Engineers make use of these models to set parameters to elicit proscribed behavior or to predict how a system will perform once parameters are set. For wireless communication systems, basic models for signal propagation, detection, and processing were derived from fundamental laws of physics and electro-magnetics. These basic models can be combined to create models of complex systems. This is known as an analytic approach, where there is a mathematical basis for the entire system model.

While this approach is both useful and powerful, the derived expressions can become impractical to solve even for systems of only moderate complexity. An alternative is to observe the complex system behavior over a range of parameter values directly through experimentation. Analytical expressions can then be derived that approximate the observed relationship between each parameter and the system behavior. These data-based expressions can then be used for designing parameters or predicting performance. This is known as the semi-analytic approach and it is the approach used for this research.

E. Channel Model

Channel models are mathematical functions that describe signal propagation through the environment. Given any transmit signal and a channel model, one can predict the signal observed at the receiver. The channel model links the analytical and simulation models of the communications system to real life operating scenarios by emulating the effect of the environment. A detailed explanation of channel modeling is beyond the scope of this paper, good references are 24 and 24. Because precise knowledge of every V2X scenario (e.g. location and geometry of every vehicle, building, roads, signs, etc.) is impossible, we rely on stochastic channel models. Stochastic models describe the channel in terms of random variables whose statistics are set appropriate to the scenario of interest. Stochastic channel models are as general as the data used to derive them.

This paper considered two stochastic channel models, each with different levels of generality. The expressway model 25, used for secondary validation of the throughput model derived in the sequel, was determined from data collected in controlled experiments on an expressway in Atlanta. This model's applicability is most specific to that stretch of Atlanta expressway. The canonical channel model, used to derive the analytical throughput model, is essentially a statistical average of channels at many different locations. The canonical model represents the channel at an average location, hence it will only approximate the propagation environment at a specific place like the Atlanta expressway.

F. Channel Estimation

In wireless communications the channel randomly alters the transmitted signal. This alteration is modeled as a multiplicative factor, i.e. $r=hx$, where x is the transmitted message, h is the channel coefficient, and r is the signal observed at the receiver. This equation has two unknowns, the channel h and the message x. With only a single receiver observation r it is impossible to determine either unknown separately.

In order to determine the transmitted message x, the receiver must determine the channel coefficient h. This process is known as *channel estimation*. Most often, the transmitter will send a message, called *training*, that is *a priori* known by the receiver. The receiver may estimate the channel coefficient as $h'=r/t$ given its observation r and the known training message t. The receiver then uses this channel estimate h' to estimate subsequent transmitted messages as $x'=r/h'=xh/h'$.[1]

As long as the estimate channel h' is effectively equal to the actual channel h, $x'=x$ and the receiver will be able to successfully determine the transmitted message. Many wireless standards, including IEEE 802.11p, prepend a training message to transmitted data in each packet to facilitate channel estimation. Typical receivers estimate the channel using this training *preamble* and utilize this estimate to decode the successive message. This processing procedure assumes that the channel estimated during the preamble is the same as that which affects subsequent data. Receivers that make this assumption are called *non-tracking* receivers. In contrast, *tracking* receivers re-estimate the channel repeatedly over the duration of a packet, often at the expense of increased receiver complexity and cost. The channel estimated at the start

[1]The prime symbol as in x' denotes an estimate of x. If $x'\neq x$ the message is received in error.

of a packet by a non-tracking receiver will not update as the time-varying channel changes over the duration of the packet. Thus, *channel estimation error*, the difference between the actual channel and the estimate, will increase with time, causing increased packet reception errors.

G. Throughput

We define throughput R as the rate of successful data reception. Throughput is proportional to the physical layer (PHY) data rate C. IEEE 802.11p supports eight transmission modes corresponding to eight PHY data rates, each proportional to the channel bandwidth. For the standard channel bandwidth, 10 MHz, the PHY data rates are 3, 4.5, 6, 9, 12, 18, 24, and 27 Mbps. Throughput accounts for transmission overhead, thus $R \leq C$. The two types of overhead considered in this research are per-packet overhead and re-transmission overhead.

Per-packet overhead consists of PHY headers and media access control (MAC) delays. PHY headers consist of training (e.g. for channel estimation) and meta-data (e.g. PHY data rate and packet length) that the receiver uses to control its decoding of the packet data. These fixed length PHY headers are prepended to the data portion of the packet as the packet *preamble.* The MAC coordinates use of a shared channel by many users. It ensures that only one user transmits over the channel at a particular time, preventing interference and improving reception rate. However, the coordination function of the MAC is not free, thus some time must be spent computing the transmission schedule. The per-packet overhead rate factor α is the percentage of the total packet duration that data is transmitted. Let T_H be the packet header duration in seconds, T_P the packet data duration, and T_M the MAC delays, then $\alpha = T_P/(T_P+T_H+T_M)$.

When a receiver cannot successfully receive a packet, it may indicate the error to the transmitter who then re-transmits the same packet. These re-transmissions do not contain any new data and thus constitute overhead. The re-transmission overhead rate factor β is a non-linear function of the packet error rate. Its computation will be described in the sequel.

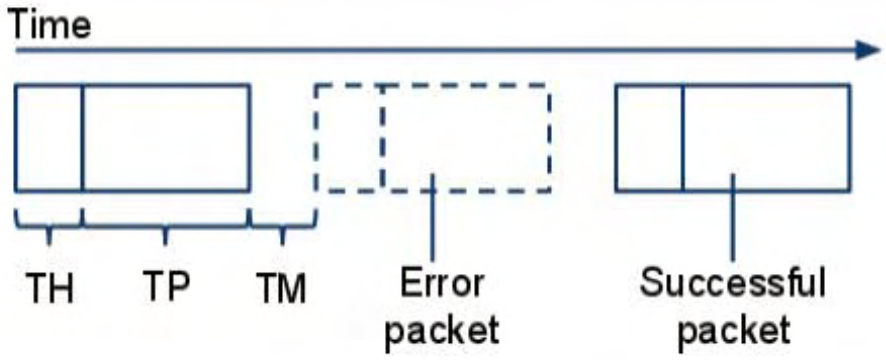

Figure 1: Delay diagram of three transmitted packets with one received in error.

H. Problem scenario

This paper considers a typical, non-tracking IEEE 802.11p system operating in a time-varying channel. Only four of the eight PHY data rates are considered: 3, 6, 12, and 24 Mbps. These rates correspond to to the nominal 10 MHz signal bandwidth and specific symbol

modulations binary phase-shift keying (BPSK), quadrature phase-shift keying (QPSK), 16-ary quadrature amplitude modulation (16QAM), and 64-ary quadrature amplitude modulation (64QAM), respectively. Many results in the sequel do not depend on the signal bandwidth and thus are labeled only with their corresponding modulation.

I. Packet Error Rate

The IEEE 802.11p system was simulated with the canonical channel model. The coherence time for the channel ranged from 16 to 320 μs.[2] Simulations were run until the minimum of 400 packet errors or 10000 transmitted packets. To ensure that channel affects dominated the performance, high SNR (30 dB) was assumed.

Figure 2 shows the simulation results for a single coherence time. The "X" marks on the BPSK and QPSK lines shows the packet length (bytes) corresponding to a packet duration equal to the coherence time. There are no X's on the 16QAM and 64QAM lines because the largest packet length simulated resulted in a packet duration less than the coherence time (i.e. all of these packets were shorter than the coherence time).

[2]At the operating frequency of 5.9 GHz this range corresponds to 34 to 675 mph. The high speed was included to predict the asymptotic performance for short coherence times on the order of one OFDM symbol duration.

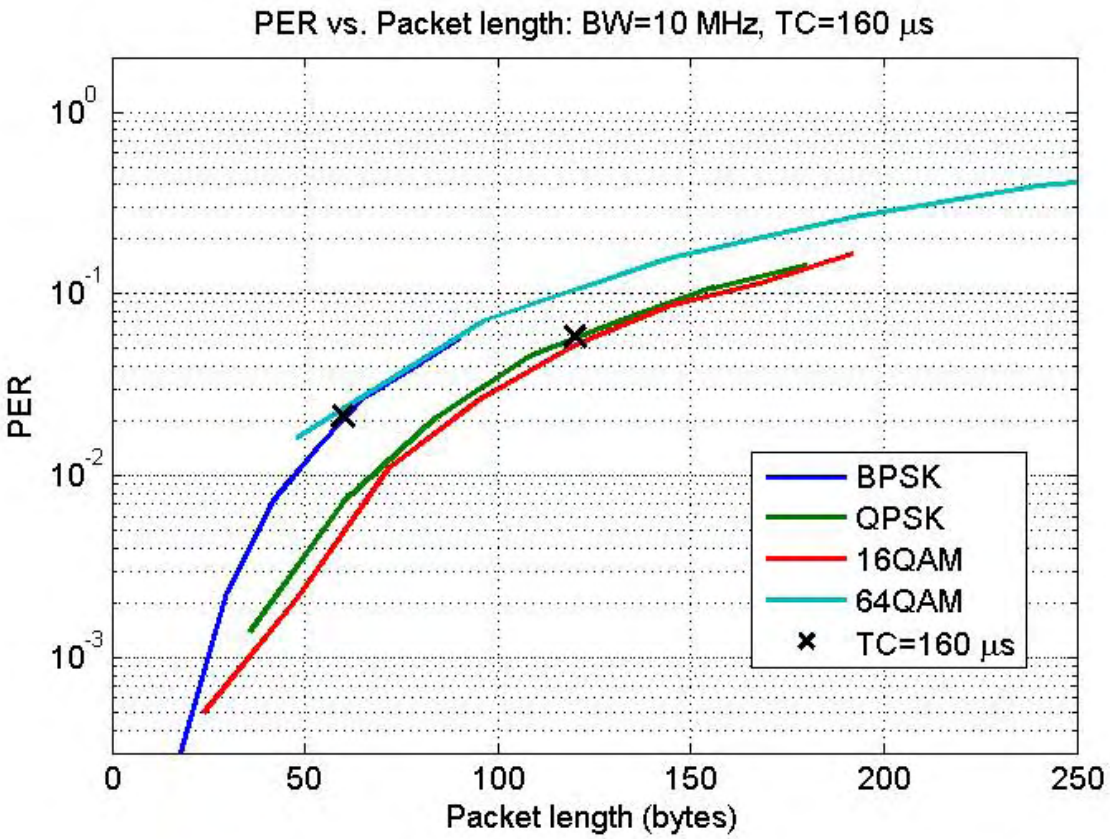

Figure 2: Packet error rate versus packet length by modulation for the 10 MHz channel.

J. Throughput

The throughput was computed as the PHY rate times the per-packet and re-transmission overhead rate factors, i.e. $R=C\times\alpha\times\beta$. The computation of the per-packet overhead rate factor α was outlined in an earlier section. The computation of the re-transmission overhead rate factor β can be understood by considering an unfair coin that lands 90% of the time on heads and 10% of the time on tails. The chance that one flips 4 tails before getting a head is: $P(4\ tails,\ 1\ head)=0.1^4\times0.9$. In general, the equation to flip N-1 tails before the first head is: $P(N\text{-}1\ tails,\ 1\ head)=p^{N-1}\times(1\text{-}p)$, where p is the probability of flipping a tail. The value N is said to be geometrically distributed and the equation $P(N)$ given is the probability mass function (PMF) of the geometric distribution. The probability that we need *at most* N flips to get one head is: $P(0..N\text{-}1\ tails,\ 1\ head)=\sum_{n=0..N-1} P(n\ tails,\ 1\ head)$ is the cumulative distribution function (CDF) of the geometric distribution. Intuitively, it's the sum of the individual probabilities that we flip a head after 0 or more tails (up to N-1). If we want to ensure that we get a head with 90% certainty, we can find the N for which the CDF is at least 0.9.

For the throughput computation, the PER corresponds to the probability of flipping a tail p and a successfully received packet is akin to flipping a head. Thus, to be 90% certain that at least one packet is successfully received, we must transmit N packets such that the geometric CDF is 0.9. In our analysis, we assume a message may be made up of K smaller packets. The procedure

remains the same except that now N is distributed according to the negative binomial distribution. This distribution generalizes the geometric distribution by giving the number of flips N, required to get K heads (or successful packets). For K=1, the negative binomial and geometric distributions are equal. Using N we computed $\beta=K/N$, the percentage of all packets transmitted that were successfully received.

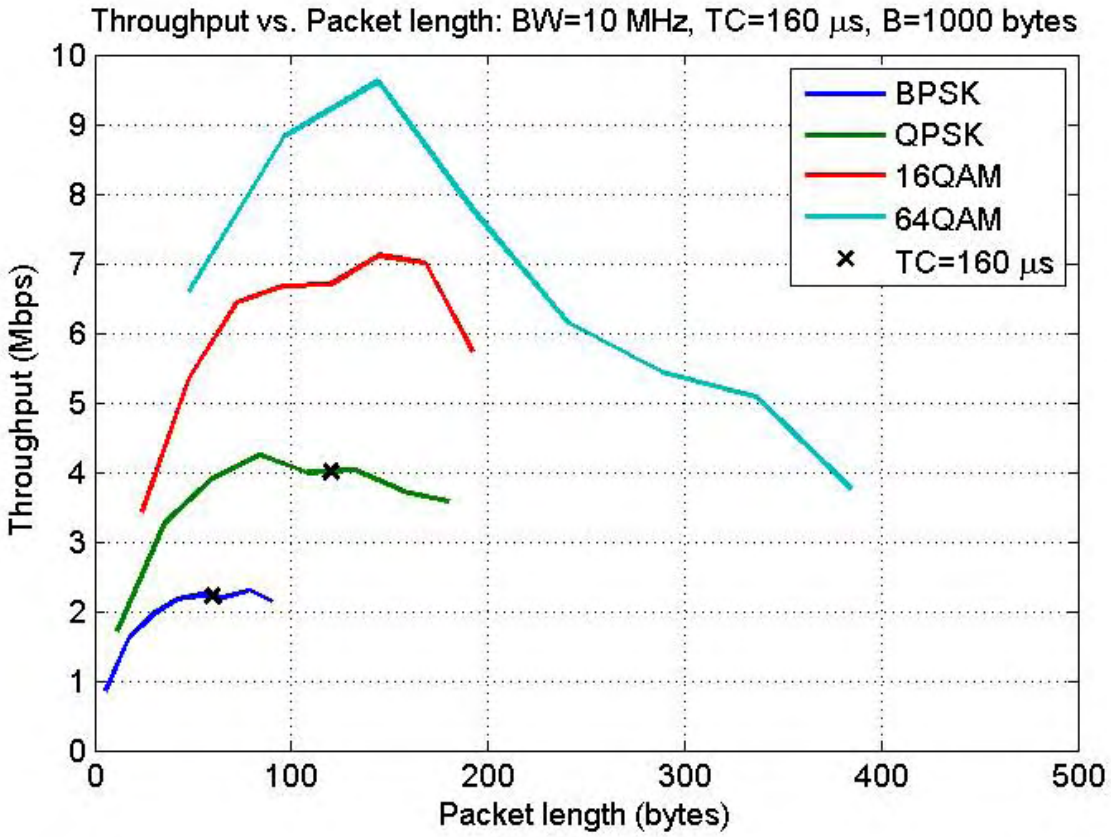

Figure 3: Throughput versus packet length by modulation for 10 MHz channel.

Figure 3 shows the transformation of the PER plots in Figure 2 to throughput. There a distinct optimal packet length corresponding to the maximum achievable throughput. The coherence time, again marked by an "X", approximates the optimal packet length only for the QPSK and BPSK modulations. The peaks in Figure 3 result from a tradeoff between per-packet and re-transmission overheads. Per-packet overhead decreases with increasing packet length (thus packet duration T_P), while re-transmission overhead increases with packet length (due to the increasing PER). For each line, per-packet overhead dominates the performance to the left of the peak (small packets), whereas re-transmission overhead dominates the performance to the right of the peak (large packet).

K. Semi-analytic model

The per-packet overhead α has a tractable, closed form expression in terms of packet duration. The same cannot be said of the re-transmission overhead β, which depends non-linearly on the packet duration according to the PER. Figure 4 is a scatter plot of the bandwidth

normalized throughput versus the coherence time normalized by the packet duration. The throughput for this plot was computed as $C/BW \times \beta$, which is the effective throughput in a 1 Hz channel. Because throughput is proportional to the channel bandwidth, it was normalized out of the equation in order to fairly compare results for different channel bandwidths. On the horizontal axis, we scaled the coherence time in units of packet durations. Because packet duration is inversely proportional to channel bandwidth, this scaling places points whose coherence time is, for example, twice the packet duration at the same abscissa. Finally, since we are only concerned with the overhead due to re-transmissions, we set the per-packet overhead α to 1.

The plot shows distinct trends for each modulation. A dotted trend line was constructed by a non-linear fitting of the data to the following function of the normalized coherence time x,

$$f(x;\vec{v}) = \frac{v_1}{\frac{v_1}{v_4} + \exp(-v_2 x)} + v_3 \tag{1}$$

where $v=\{v_1,v_2,v_3,v_4\}$ is a four element parameter vector and $exp(x)=e^x$. This function is a generalization of the hyperbolic tangent function, an S-shaped function similar to the trends evident in the scatter plots.

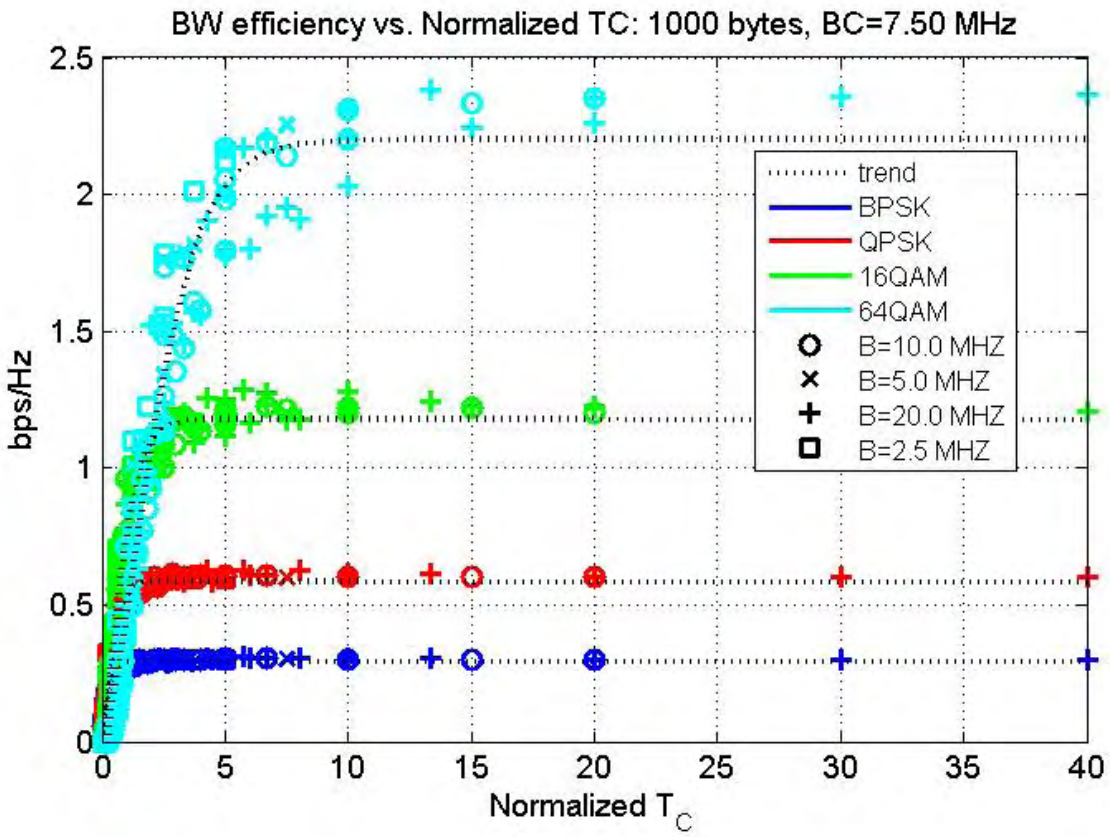

Figure 4:Bandwidth normalized throughput vs. normalized coherence time exposes the trends for each PHY modulation.

The parameters for each trend line of Figure 4 are given in Table 1.

Modulation	v_1	v_2	v_3	v_4	Corner	Plateau
BPSK	1.44	4.56	-0.48	0.78	0.57	0.29
QPSK	1.14	3.19	-0.62	1.21	0.95	0.59
16QAM	1.87	1.75	-1.13	2.31	1.80	1.18
64QAM	1.41	0.76	-1.11	3.30	4.59	2.20

Table 1: Trend line parameters with corner and plateau measurements.

These four functions constitute the analytical models relating throughput and packet length given the channel coherence time, channel bandwidth, and PHY data rate. The table contains two measures based on the analytical models. The *plateau* is the ordinate of Figure 4 at which the trend line becomes flat. This occurs when the channel is effectively static. Theoretically the plateaus should be *C/BW*, that is 0.3, 0.6, 1.2, and 2.4 for BPSK, QPSK, 16QAM, and 64QAM, respectively. The *corner* is the abscissa for which the ordinate is 90% of the plateau. It demarcates the normalized coherence time which results in at 90% of the maximum potential throughput. For example, a packet transmitted with 64QAM symbols must be at least 4.6 times

shorter than the coherence time to achieve at leaset 90% of the PHY data rate. For BPSK, on the other hand, the packet can be as long as 1/0.57=1.75 times the coherence time and maintain 90% of the peak data rate. We refer to the corner as the *normalized empirical coherence time (NETC)*. Given the channel coherence time T_C, the packet duration predicted to achieve 90% of the peak throughput can be computed as $T_C/NETC$.

L. Model validation

The achievable throughput predicted by the models was validated against a number of results from simulation using the canonical channel model. The dotted "fit" lines in Figure 5 along with the NETC-based packet duration (□ symbol) show good agreement with the simulation results. The dashed lines and coherence time marks (O symbol) show the throughput and optimum packet length, respectively, predicted by conventional analysis which ignores re-transmission overhead.

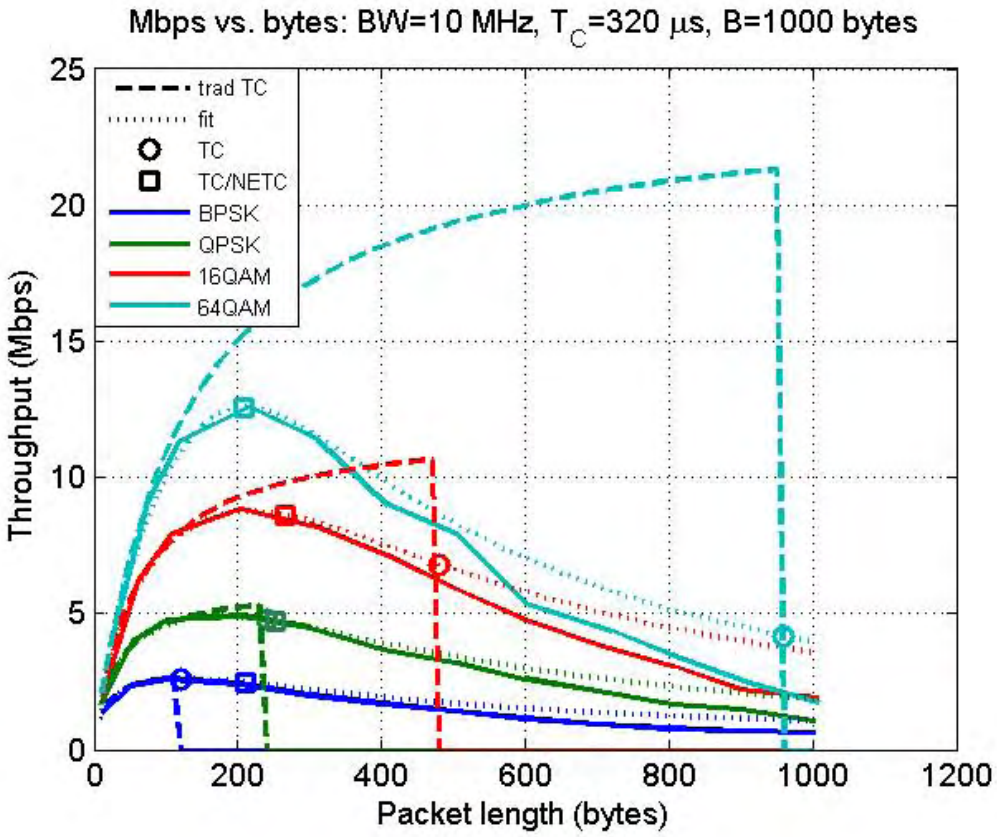

Figure 5: Throughput versus packet length for the system operated over the canonical channel.

Our semi-analytic model was derived from simulated system performance over the canonical channel with varying coherence time. Figure 5 suggests that our model predicts throughput performance well for the class of channels that share the same structure as the canonical channel but have arbitrary coherence times. Our second validation compared the predicted throughput performance to simulated system performance over the more realistic expressway channel.

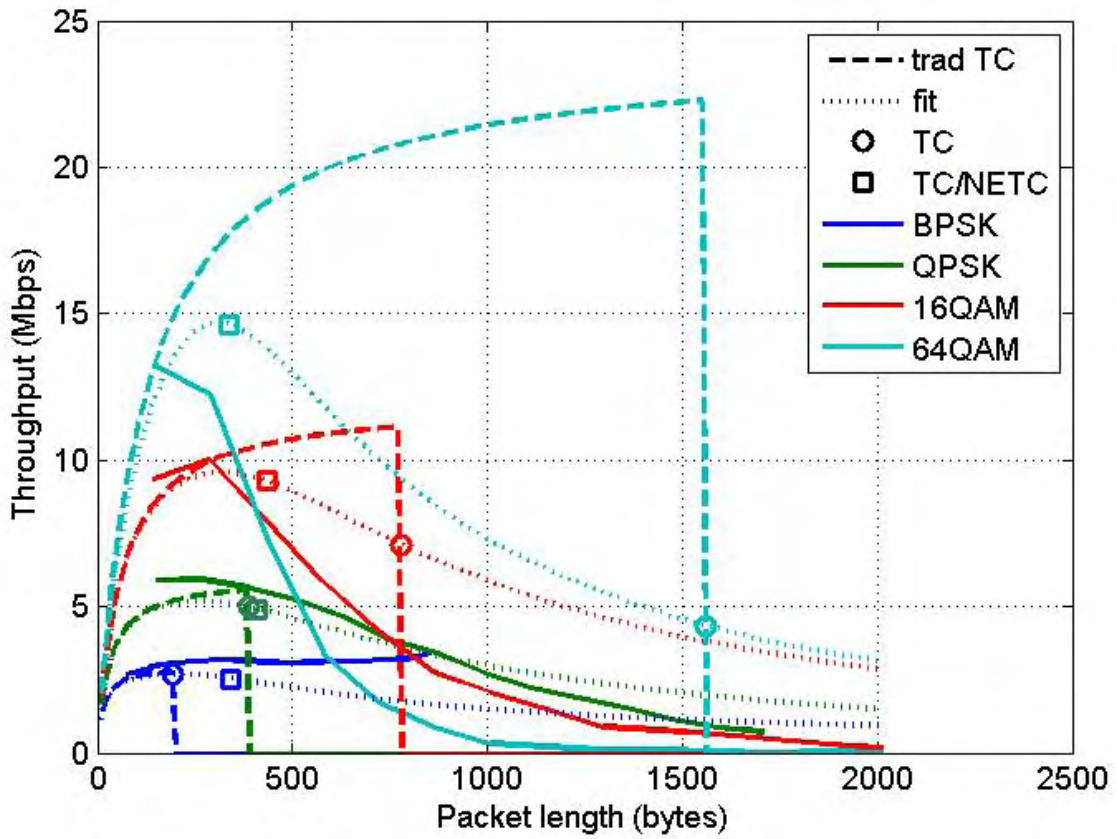

Figure 6: Throughput versus packet length for a system operated over the expressway channel.

Figure 6 is identical to the previous figure except that the simulated results (solid lines) are for a system operated over the expressway channel. The predicted throughput now only approximates the simulated throughput. The NETC-derived maximum packet length (□ symbol), while somewhat optimistic, is still much more predictive of the optimal packet length than that derived from the basic coherence time (O symbol).

M. Channel bandwidth comparison

The analysis in this section compares the theoretical maximum achievable throughput versus channel coherence time for transmissions at fixed PHY rates with channels of varying bandwidth. Given a channel coherence time T_C, PHY data rate, bandwidth, and MAC overhead T_M the optimal packet length was computed by finding the maximum of the throughput versus packet length function (e.g. the peak of the "fit" lines in Figure 5). The MAC overhead T_M was set to zero, thus the given throughput values upper-bound the throughput for any practical MAC.

In order to fairly compare two bandwidth options the underlying PHY data rate must be equal. For single channel options, the transmit modulation was used to compensate for the data rate disparity due to differing bandwidths. For example, in Figure 7 the 24 Mbps rate uses 16QAM modulation for the 20 MHz channel and 64QAM for the 10 MHz channel. Comparing

single channel operation in both Figure 7 and Figure 8 shows a loss in potential throughput using smaller bandwidth channels. This loss is greatest for the highest PHY data rates.

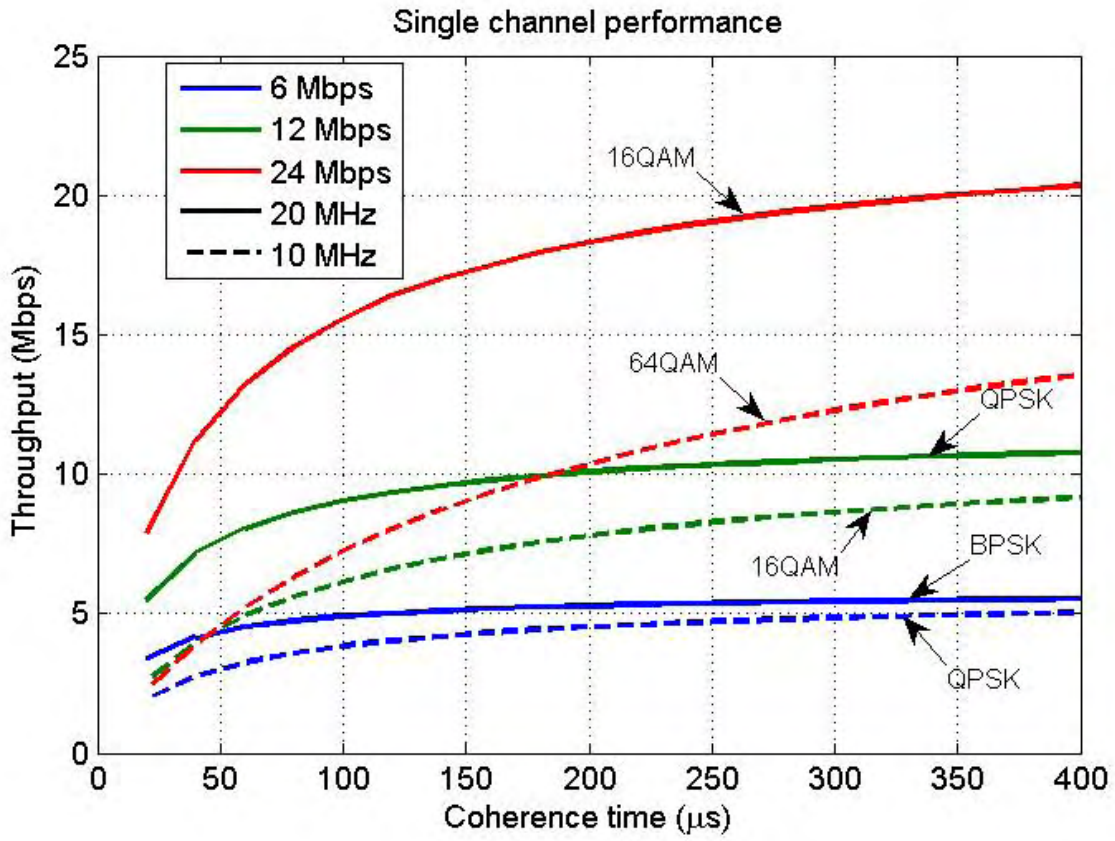

Figure 7: Single channel comparison of 10 MHz and 20 MHz channel throughput.

Alternatively we can maintain the overall signal bandwidth and transmit modulation by considering multiple smaller channels within a larger bandwidth. For example, we can compare the performance of a single 20 MHz channel to two 10 MHz channels as in Figure 9. In this figure as well as Figure 10, there is again a throughput degradation when operating over smaller bandwidth channels. However, the degradation is less pronounced than the single channel case.

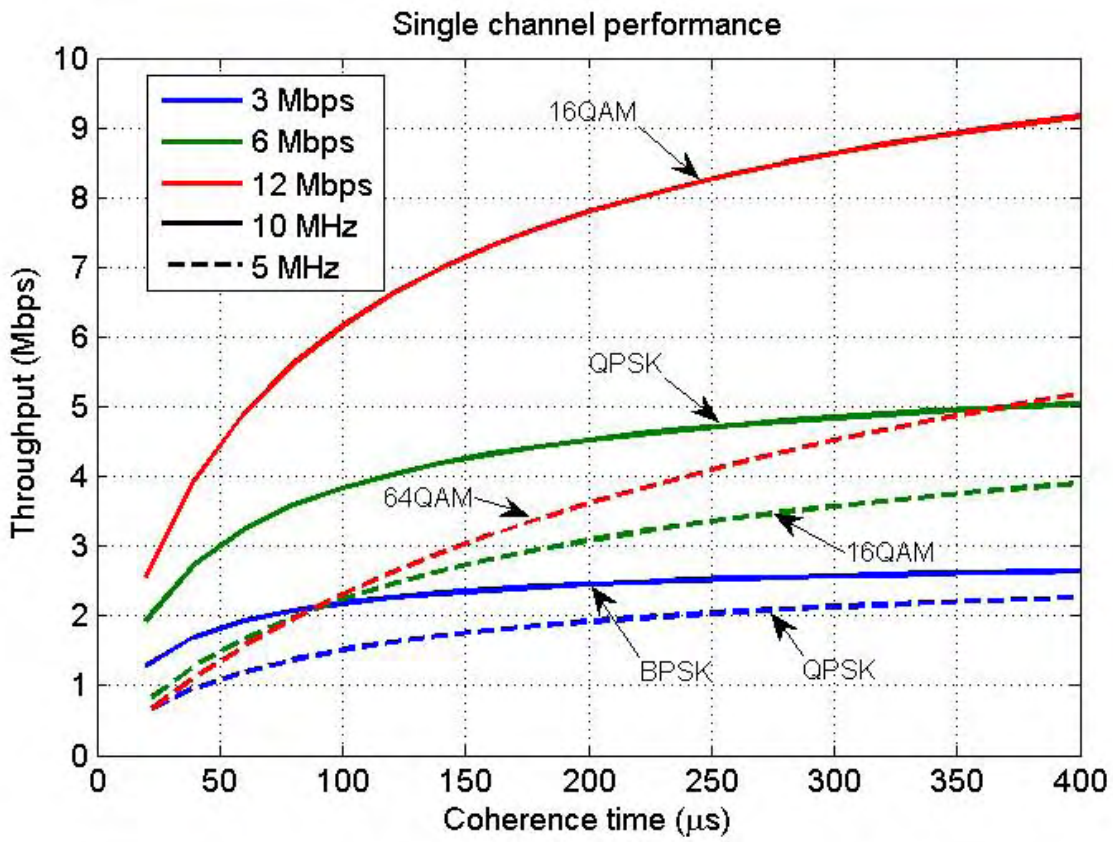

Figure 8: Single channel comparison of 5 MHz and 10 MHz channel throughput.

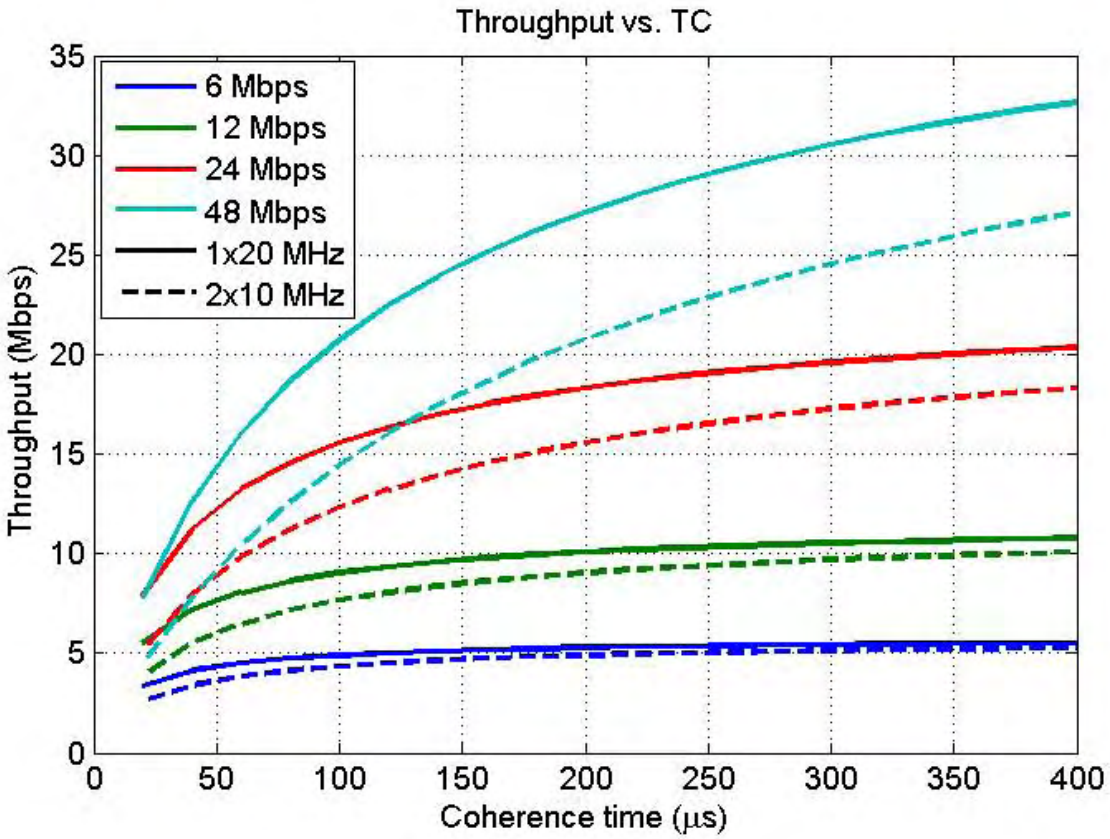

Figure 9: Comparison of the achievable throughput of one 20 MHz channel or two 10 MHz channels.

N. Conclusions

This research quantified the achievable throughput of bandwidth scaled IEEE 802.11p operated over time-varying channels. A semi-analytic model was derived relating bandwidth normalized throughput to coherence time normalized to the packet duration for a class of channels (the canonical channels). We showed that this model accurately predicted the optimal packet length for operation over channels within the canonical channel class, while it only approximated the optimal packet length for a specific channel (the expressway channel) not part of the canonical class. This suggests that the coherence time is an insufficient statistic to describe a channel.

The semi-analytic model was used to compare the throughput potential of a number of channel bandwidth alternatives. In time-varying channels, signals with greater bandwidth achieve greater throughput than those with less bandwidth. This conclusion is intuitive since packets of a particular length sent over channels with greater bandwidth have a shorter duration in time and thus experience less channel variation which results in reduced channel estimation error and greater error rate performance.

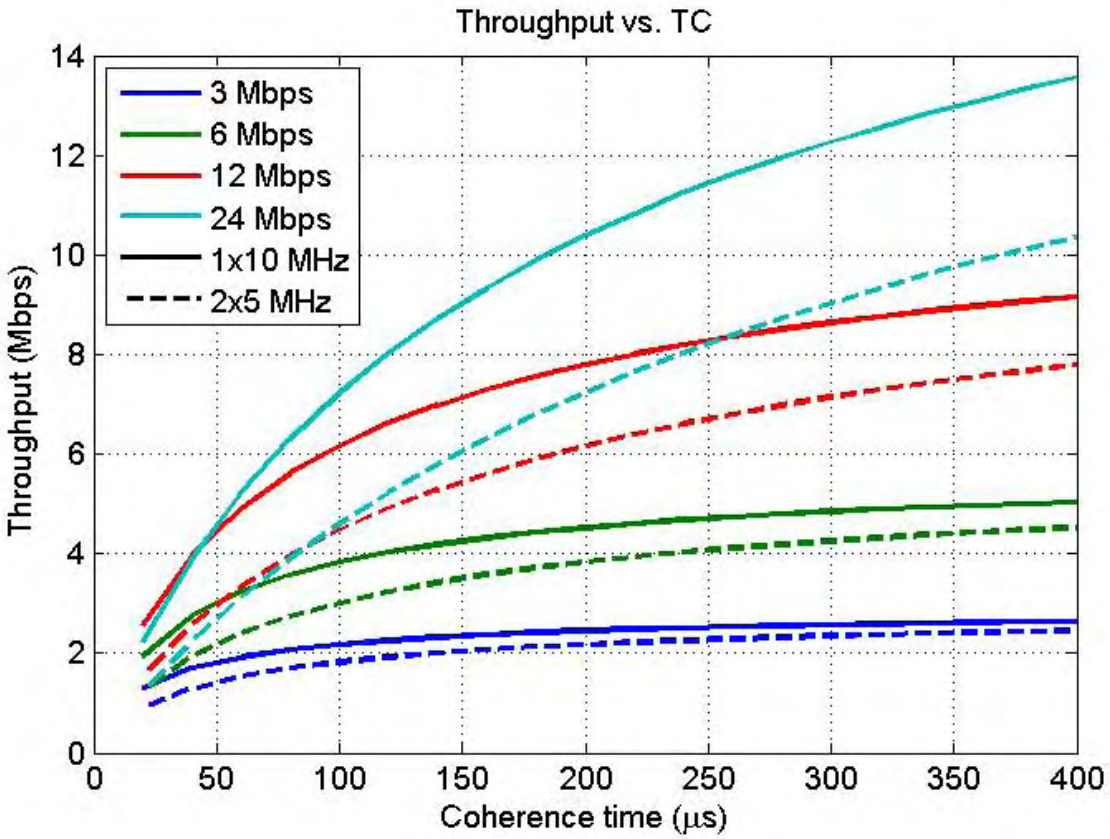

Figure 10: Comparison of the achievable throughput of one 10 MHz channel or two 5 MHz channels.

O. References

[1] "Part 11: Wireless LAN Medium Access Control (MAC) and Physical Layer (PHY) specifications: Amendment 3: Wireless Access in Vehicular Environments (WAVE)," IEEE P802.11p/D1.0, Feb. 2006.

[2] Charan Langton, "Orthogonal Frequency Division Multiplex (OFDM) Tutorial," Intuitive Guide to Principles of Communications, 2002, retrieved online Dec. 2010, http://www.complextoreal.com/chapters/ofdm2.pdf.

[3] Stephen B. Weinstein, "The History of Orthogonal Frequency-Division Multiplexing," IEEE Communications Magazine, Nov. 2009.

[4] J. Dulmage, M.P. Fitz, D. Čabrić, "A Modulation Dependent Channel Coherence Metric for VANET Simulation using IEEE 802.11p," IEEE VTC Spring, May, 2010.

[5] Ana Aguiar and James Gross, "Wireless Channel Models," Technical Report, Technical University of Berlin: Telecommunications Networks Group, April, 2003.

[6] Bernard H. Fleury and Peter E. Leuthold, "Radiowave Propagation in Mobile Communications: An Overview of European Research," IEEE Communications Magazine, Feb. 1996.

[7] G. Acosta, M. A. Ingram, and K. Tokuda, “Measured joint Doppler-delay profiles for vehicle-to-vehicle communications at 2.4 GHz,” in proceedings, IEEE GLOBECOM, vol. 6, Dec. 2004, pp. 3813—3817.

III. Network Performance Analysis in NS-2

A. Network Simulator (NS-2)

NS-2 is an open source simulator commonly utilized in networking research because it allows researchers to easily extend and modify the source code for their particular application. In 2007, Jiang et al. released an NS-2 patch with new implementations of the Physical (PHY) and Medium Access Control (MAC) layers to model real world environments more accurately [1]. The latest NS-2 release (ns-2.34) includes their work as the "ns-2-802.11Ext" module [2]. We chose to work with NS-2 because of the easy access to the source code and documentation of the 802.11Ext module.

We simulated a vehicular network as a group of static wireless nodes arranged to mimic vehicles on a road. The simulation setup is illustrated in Figure 11 and was implemented as follows. The road has length L and can have one or more lanes. The nodes are placed along each lane so that the distance, d, between each consecutive node is an uniformly distributed variable with mean d_0. Let the number of lanes be denoted by n, then the number of vehicles per kilometer of road is $N = 1000n \div d$. In our simulations, $L = 1km$, $n = 4$, and d_0 was either set to *5m (~800 vehicles per km)*, *10m (~400 vehicles per km)*, or *30m (~130 vehicles per km)*. All the nodes were set to broadcast *250byte* packets at a rate of *10 packets per second*.

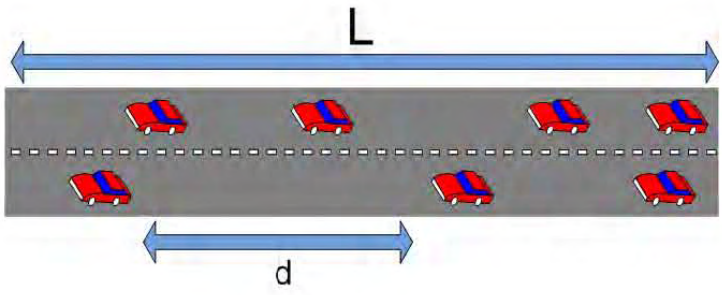

Figure 11: Vehicular network simulation scenario

B. Background

1. Signal-to-Noise Ratio (SNR)

We want the communication system to be as efficient as possible, i.e. every bit transmitted is correctly received so no retransmission is necessary. In other words, we would like to minimize the probability of errors occurring. It can be shown that *Signal-to-noise ratio (SNR)* is inversely related to *Bit Error Rate (BER)*, i.e. higher SNR means lower BER, and lower SNR means higher BER. Thus, for the maximum efficiency, we must design the communication system so SNR is maximized.

SNR is defined as the ratio of signal power to the noise power, i.e. how much the transmitted signal has been corrupted by noise. There are mechanisms for decreasing noise, but this leads to increased complexity and cost of the receiver. Given these constraints, it is generally assumed that the noise can only be reduced to a certain level, called the noise floor. Alternatively, we may

increase the transmitted signal power. Similar to decreasing noise, increasing the transmit power is also limited. Thus, we see that only a maximum SNR is achievable. In conclusion, given specific transmitter and receiver characteristics, we can only achieve an optimum SNR.

2. Signal Power vs. Distance

Intuitively, we expect that the greater the distance between the transmitter and receiver the more likely errors are to occur. The role of distance in determining SNR is explained by path loss. *Path loss*, or *attenuation*, is the difference between the transmitted signal power and the received signal power due to the physical properties of electromagnetic propagation. Even in the idealized case of *free space* (when there are no other objects besides the transmitter and the receiver, and they are both in a vacuum), the received power will only be a fraction of the transmitted power. The received power, P_{recv}, is given by the *Friis transmission equation*

$$P_{recv} = \frac{P_{tx}}{d^n}\left(\frac{\lambda}{4\pi}\right)^2 \tag{0.1}$$

where P_{tx} is the transmit signal power, d is the distance between the transmitter and receiver, n is the pathloss exponent, and λ is the wavelength of the signal, assuming unity gain for both the transmitter and the receiver. The pathloss exponent n is generally taken to be between 2 and 4 for outdoor environments. In our simulations, we used a two-segment model: for $d <= 30m$, $n = 2$, and for $d > 30m$, $n = 3$.

3. Fading

In reality, the attenuation seen by the receiver is not constant, even if the distance stays the constant. In fact, it may change with time, position, or frequency. This effect is called fading and it models the randomness of wireless communication channels. *Rayleigh fading* is commonly utilized in scenarios where it is expected that no dominant line-of-sight signal is present, for example in modeling wireless channels in urban environments. The Rayleigh model is the theoretical result for when the received multipath signal consists of many reflected waves. Some of the simulations utilized Rayleigh fading because in vehicle-to-vehicle communication scenarios the transmitter and receiver will generally not have a clear line-of-sight link. Given a Rayleigh fading model, the received power is exponentially distributed. Thus, the probability that the received power is below a specified threshold power, $P_{thrshld}$, i.e. probability that the packet cannot be received, can be calculated with the following equation

$$\Pr(P_{recv} < P_{thrshld}) = 1 - \exp\left(-\frac{P_{thrshld}^2}{2 * P_{recv}^2}\right) \tag{1.1}$$

When two vehicles are close together, there might be a strong line-of-sight component in the received signal. An example would be a highway scenario where vehicles are communicating only with their direct neighbors. In this case, the *Rician fading* model can be used. This model is the theoretical result in the case where the received signal consists of several reflected and scattered waves and there is one dominant component. The probability distribution function (PDF) of the received signal power is given by

$$f(\mathrm{P}_{recv}) = \frac{(1+K)e^{-K}}{\bar{P}} e\left(-\frac{1+K}{\bar{P}}\mathrm{P}_{recv}\right) I_0\left(\sqrt{(4K(1+K)\frac{\mathrm{P}_{recv}}{\bar{P}}}\right) \quad (1.2)$$

where K is the *Rician K-factor* (ratio between signal power of dominant component over local-mean scattered power), and is the $\bar{P}$ is the *total local-mean power* (sum of the power in the line-of-sight and the local-mean scattered power). This is called a non-central chi-square distribution. The probability of reception is calculated from the cumulative distribution function (CDF) of the power,

$$\Pr\left(\mathrm{P}_{recv} < P_{thrsh}\right) = 1 - Q\left(\sqrt{\lambda}, \sqrt{x}\right) \quad (1.3)$$

where $\lambda = 2 \cdot \frac{P_{recv}}{\bar{P}}(1+K)$ and $x = 2K$.

The Nakagami fading model has been found to better match empirical results compared with Rician model [7]. The Nakagami PDF and CDF are given below [8].

$$f(d;\mu,\omega) = \frac{2\mu^{\mu}}{\Gamma(\mu)\omega^{\mu}} d^{2\mu-1} \exp\left(-\frac{\mu}{\omega}d^2\right) \quad (1.4)$$

$$F(d;\mu,\omega) = P\left(\mu, \frac{\mu}{\omega}x^2\right) \quad \textit{where P is the incomplete gamma function (regularized).} \quad (1.5)$$

In our simulations, we first utilized Rayleigh fading and then later, for short range scenarios, the Nakagami model. The results of all simulations are presented in Section III.

4. Probability of Reception vs. Distance

Using **Equations 2.1** and **3.1**, we can determine the theoretical probability of reception, P_r, versus distance. This reliability metric is calculated from the transmit power and a specified threshold power. **Equation 2.1** allows us to calculate the received signal power, P_{recv}. Then, using **Equation 3.1**, we account for fading and get the probability of reception. The threshold power is determined from the desired SNR and the noise floor. For example, let the SNR needed for reception of a BPSK signal be 5dB, and the noise floor be -90dBm, then $\mathrm{P}_{\mathrm{thrshld}}$ = -90+5 = -85 dBm . Figure 12 below shows the probability of reception curve for transmit power of 23dBm and threshold power of -85dBm.

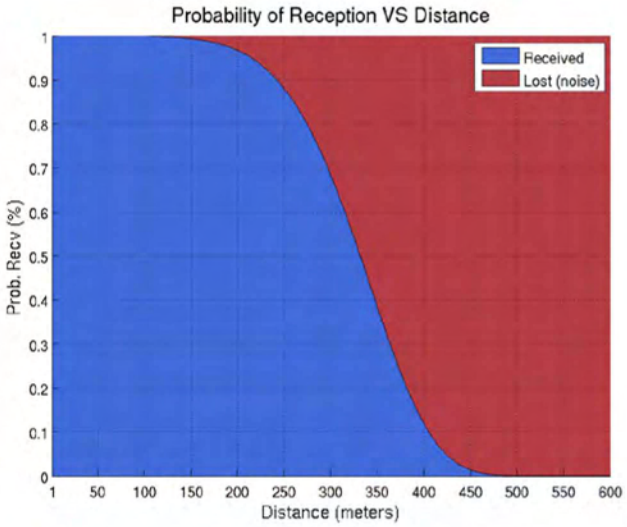

Figure 12: Prob. of reception for P_{tx} *= 23dBm and* $P_{thrshld}$ *= -85 dBm*

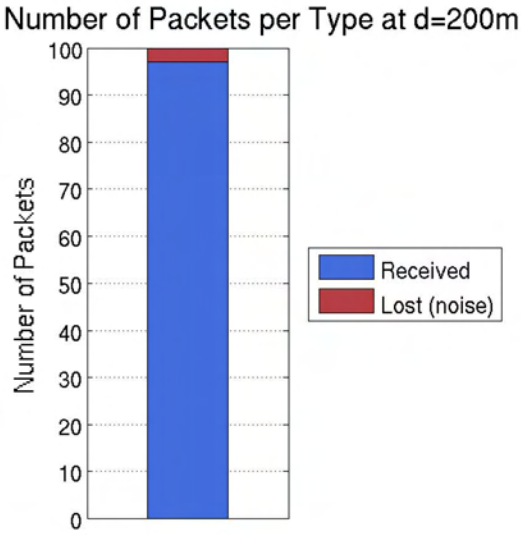

Figure 13: Example 1 bar plot

Example 1

Let's assume the distance between the transmitter and the receiver is 200 meters. Then from the curve shown in Figure 12, we expect that if we transmit 100 packets, we will correctly receive 97 packets and 3 packets will be lost. This is illustrated in Figure 13 to the left. Note that for any given distance a similar bar plot can be derived from the curve in Figure 12.

This *Prob. of Reception vs. Distance curve* enables us to answer questions about expected reliability and range. For example, if we want to have a completely reliable system, that is the probability of reception is 100%, then our range is about 100 meters. However, the range increases to about 190 meters if we can tolerate some packet loss, i.e. need only 90% reliability. Of course, we can also determine how reliable the communication system is given a specific range. For example, at 300 meters, we only expect to receive 20% of the transmitted packets.

5. Interference

In a typical V2V scenario, there are many nodes trying to communicate at the same time. Intuitively, we can guess that the contention amongst the nodes will affect performance of the communication system. For example, node A is transmitting a packet to node B. As we know, the distance between the two nodes and the fading characteristics of the channel will affect the

SNR and the probability of reception. Now, let's assume that node C is transmitting at the same time as node A, and that node C is within the reception range of node B. Thus, node B "hears" the transmission from both node A and node C simultaneously. Node B is trying to receive node A's message, so node C's signal can be considered added noise, which we call *interference*.

Interference caused by multiple transmitted signals in the same frequency band, or channel, is called *Co-Channel Interference (CCI)*, and interference due to signals in other frequency bands is called *Adjacent Channel Interference (ACI)*. Here, we will analyze the effect of CCI and assume that ACI is handled by adequate filtering and channel management.

The *Signal-to-Interference Ratio (SIR)* is defined as the ratio between the transmitted signal power and the sum of all the interfering signals' power, which we will call interference power. As can be expected, SIR is inversely related to BER, and system performance is improved by increasing SIR. The instantaneous interference power, P_I, is the sum of the powers of all interfering signals at that moment and is equivalent to the concept of noise floor. We can calculate a threshold power from P_I and SIR just like in the previous section. This will give us curves just like the one shown in Figure 12.

We want our model to account for interference in addition to pathloss and fading. To achieve this, we combine SNR and SIR in a third metric, *Signal-to-interference plus noise ratio (SINR)*. SINR is defined as the ratio between the transmit signal power and the sum of the noise plus interference powers. As with SNR and SIR, we can plot a probability of reception vs. distance curve for SINR as well. By plotting this curve on the same plot as Figure 12, we can analyze the effects on the probability of reception due to noise and interference (see Figure 14 and ***Example 2*** on the next page).

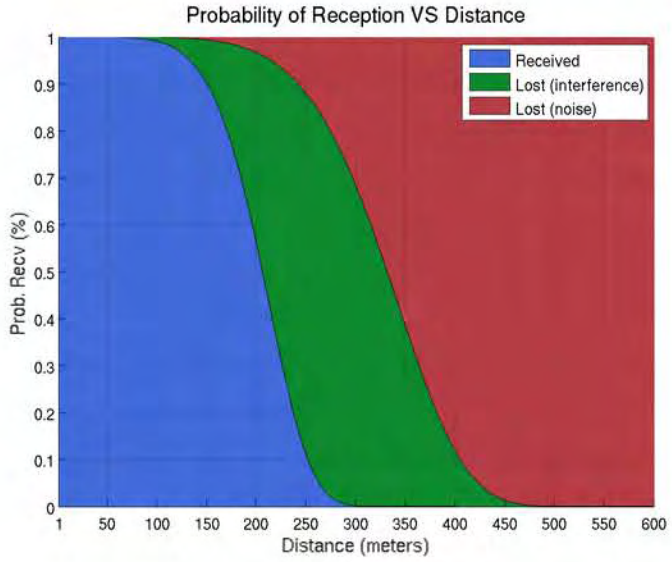

Figure 14: Prob. of reception accounting for path loss, fading, and interference

(P_{tx} *= 23dBm,* $P_{thrshld}$ *= -85 dBm,* noise floor *= -90dBm,* P_I *= -5dBm)*

Example 2

Let's again assume the distance between the transmitter and the receiver is 200 meters. Just like in ***Example 1***, for any given distance a bar plot can be derived from the curves shown in

Figure 14. If we transmit 100 packets, we will correctly receive 56 packets (blue area) and 44 packets will be lost. The bar plot for d=200m is shown in Error! Reference source not found.. Note that the number of packets lost because the receiver is out of range (red area) is the same as in ***Example 1***. However, because of interference many additional packets are lost (green area).

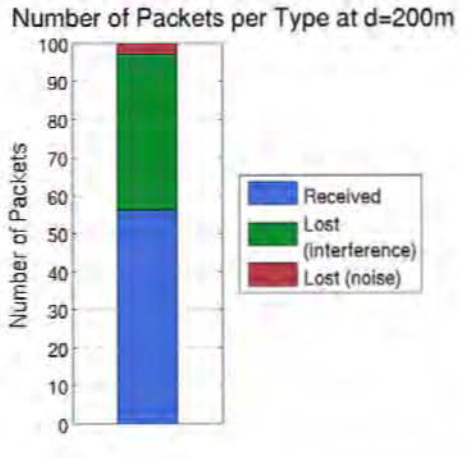

Figure 15: Example 2 bar plot

C. Simulation Results

1. Probability of Reception vs. Transmit power and Vehicle density

Recall from Sections I.2 and I.3 that the probability of reception of a packet is related to the received power, P_{recv}, which in turn is proportional to the transmit power, P_{tx}. Thus, we can change the probability of reception curve of the system by controlling P_{tx}. We experimented with two levels of P_{tx}, "low power" was 0 dBm, and "high power" was 23 dBm.

Recall from Sections I.5 that the level of interference also affects the probability of reception. Higher vehicle density means there will be more nodes within range of each receiver; clearly this increases the chance of multiple nodes transmitting at the same time. Additionally, the smaller distance between nodes leads to higher interference between nodes, because interference power is inversely proportional to distance. Therefore, we can simulate various vehicular scenarios by simply changing the vehicle density. As stated previously, we ran simulations for scenarios with vehicle separation d=30m (low density), 10m (medium density), and 5m (high density).

Figure 16 and Figure 17 show the simulation results for the low vehicle density scenario with both low and high transmit power respectively. Note that the range with high power is much greater than with low power. For example, at 90% reception rate, we have a significantly larger range, about 80m, with high power compared to about 15m with low power. In low density scenarios, it's better to transmit with high power to achieve greater range, since interference does not increase significantly.

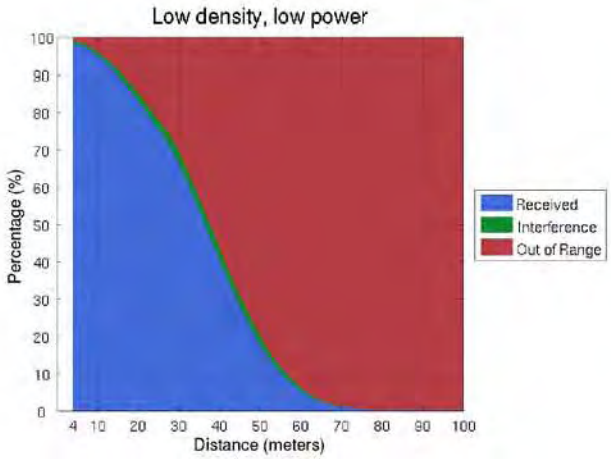

Figure 16: d=30m, P_{tx}=0dBm, single 250B packet

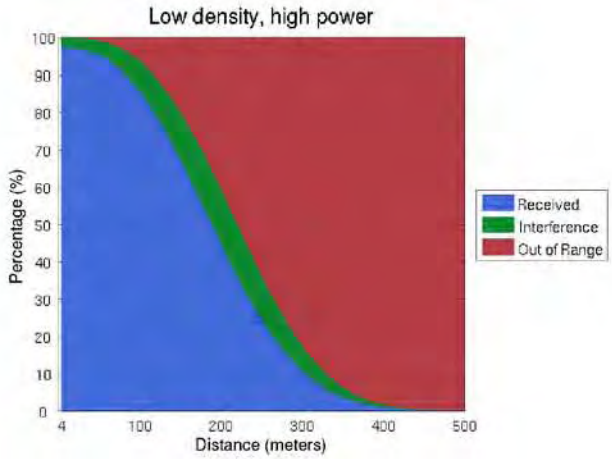

Figure 17: d=30m, P_{tx}=23dBm, single 250B packet

Results for medium vehicle density are shown in Figure 18 (low power) and Figure 19 (high power). Note that interference levels become significantly worse in the high transmit power scenario. Again, this is due to the increased number of vehicles transmitting within the reception range of the receiving nodes. However, it can be seen that system performance is still better in the high power case over low power. For example, at 80% reception rate, we see a reception range of about 55m with high power and only 20m with low power. Therefore, we conclude that even though interference levels are much worse with high transmit power, the system performance may still be superior than with low transmit power.

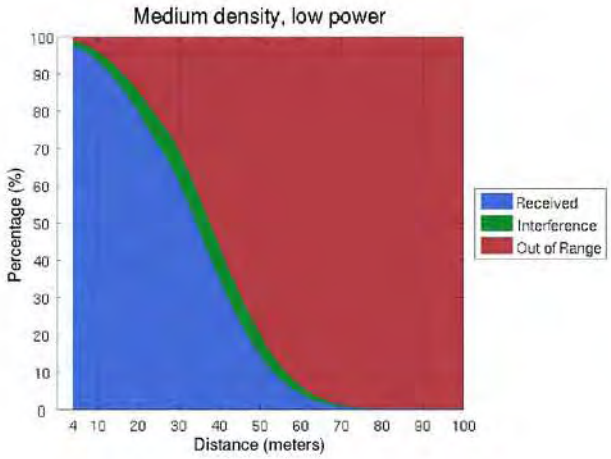

Figure 18: d=10m, P_{tx}=0dBm, single 250B packet

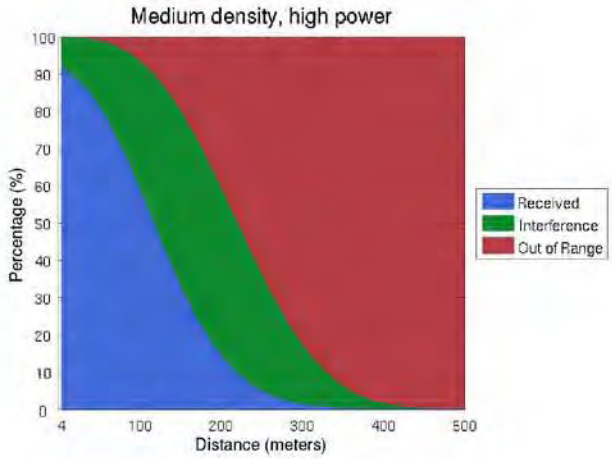

Figure 19: d=10m, P_{tx}=23dBm, single 250B packet

As expected, interference level escalated as vehicle density increased. In fact, system performance became unsatisfactory in the high vehicle density, high transmit power scenario, as shown in Figure 21. Results show that even an 80% reception rate (too low for safety applications) can only be achieved up to a distance of 8m (corresponding to vehicles in the immediate vicinity of the transmitter). The "transmitting" category indicates the number of packets dropped because the receiver was transmitting at the time a packet arrived. A node cannot receive and transmit at the same time, so the packet was dropped. Figure 20 shows the results for the low transmit power case. Note that 80% reception is achieved up to a range of

16m. This is a smaller range than in the medium density scenario, but performance is not as adversely affected in the low power cases (Figure 18 and Figure 21) compared to the high power cases (Figure 19 and Figure 21).

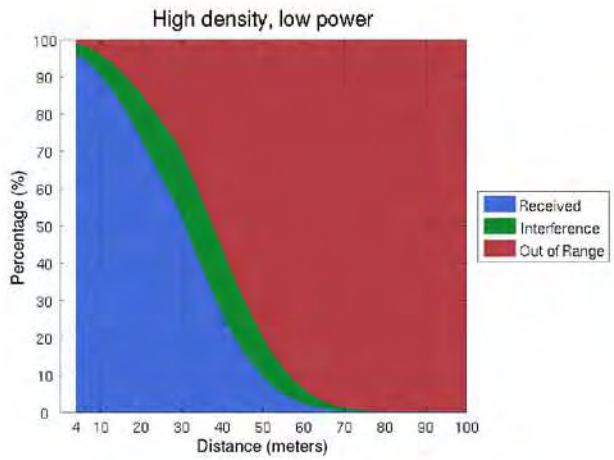

Figure 20: d=5m, P_{tx}=0dBm, single 250B packet

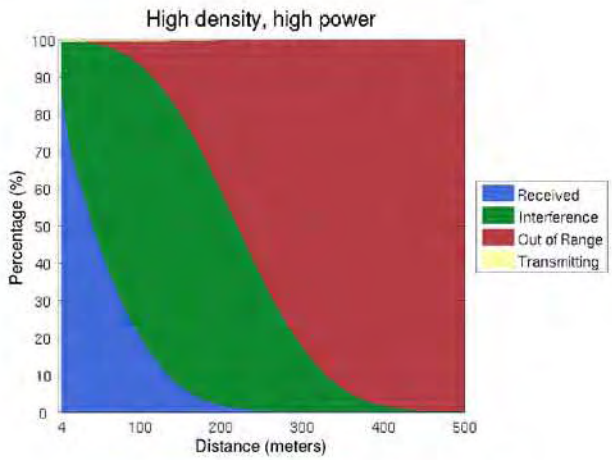

Figure 21: d=5m, P_{tx}=23dBm, single 250B packet

2. Probability of Reception vs. Packet size

We also ran simulations with different packet sizes. Results shown in Section II.1, had nodes transmitting 10 packets/second, each of size 250 bytes. This yields a data rate of 2.5kB per second (kbps). We also ran simulations with 100B packets, corresponding to a lower data rate of 1kbps As expected, we see decreased interference because of the lower bandwidth usage.

Indeed, this is observed in the simulation results shown below. Compare Figure 18 with Figure 22 (low transmit power), and Figure 19 with Figure 23 (high transmit power).

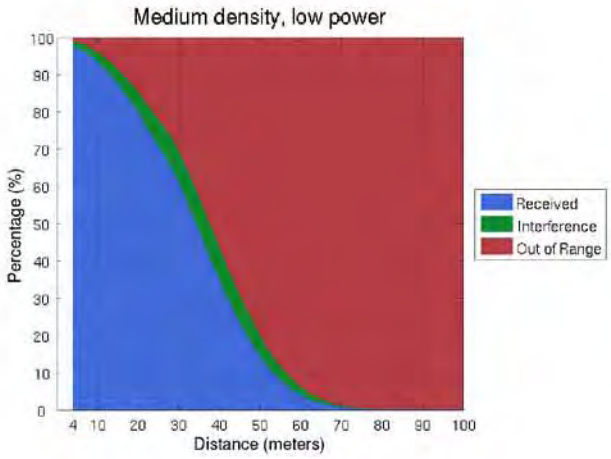

Figure 22: d=10m, P_{tx}=0dBm, single 250B packet

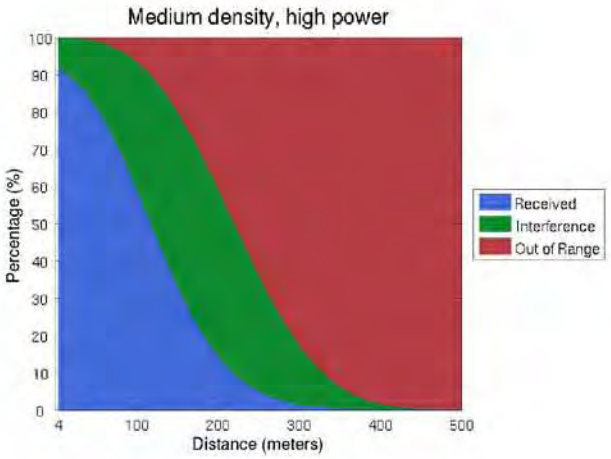

Figure 23: d=10m, P_{tx}=23dBm, single 250B packet

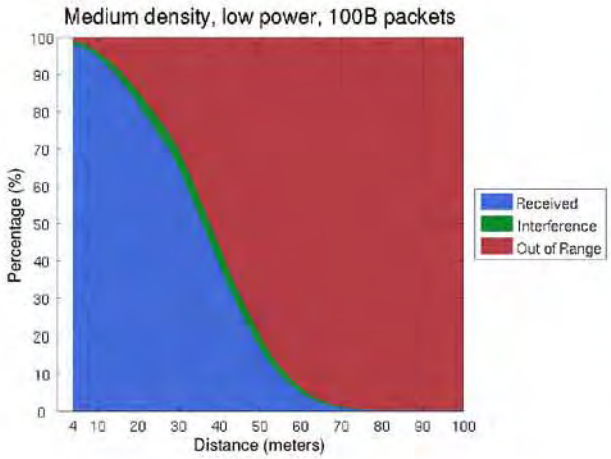

Figure 24: d=10m, P_{tx}=0dBm, single 100B packet

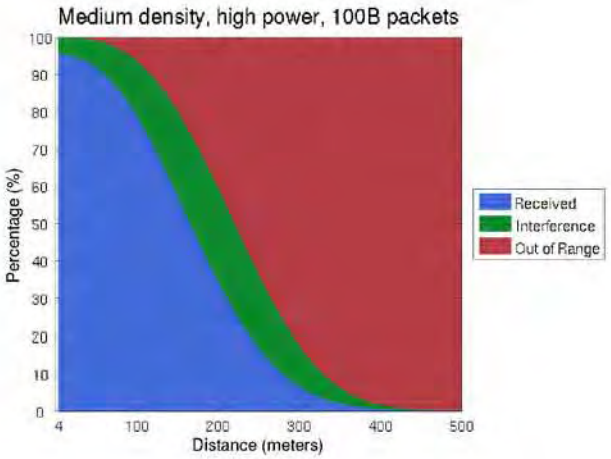

Figure 25: d=10m, P_{tx}=23dBm, single 100B packet

For a fairer comparison, we also ran simulations where the data rate was equivalent. We decreased packet size to 50B, but transmitted 50 packets per second instead of 10 packets per second. Thus, data rate was kept at 2.5kB. Figure 24 compares the two cases.

Figure 26: Illustration of transmission of one 250B packet and five 50B packets

The figure above makes clear how there's additional overhead for sending five 50B packets instead of a single 250B packet. For a given amount of data to be transmitted, we must utilize more of the channel for the headers of each packet. The increased channel usage by each transmitting node leads to greater interference levels and system performance deteriorates. The figures on the next page show that interference increased in all scenarios when nodes transmitted five 50B packets compared to transmitting one 250B packet (compare figures 16-21 with corresponding scenario results in figures 27-32).

Example 3

Let's again assume the distance between the transmitter and the receiver is 200 meters. Then from **Figure 17**, we have the bar plot shown in **Figure 25**. If we have the same traffic scenario, but with nodes transmitting five 50B packets, we get the bar plot shown in **Figure 26**. This plot is obtained from the *Probability of Reception vs. Distance* curve shown in **Figure 30**. Note the increased number of packets lost to interference. This is caused by the additional overhead of sending five packets compared to transmitting a single packet.

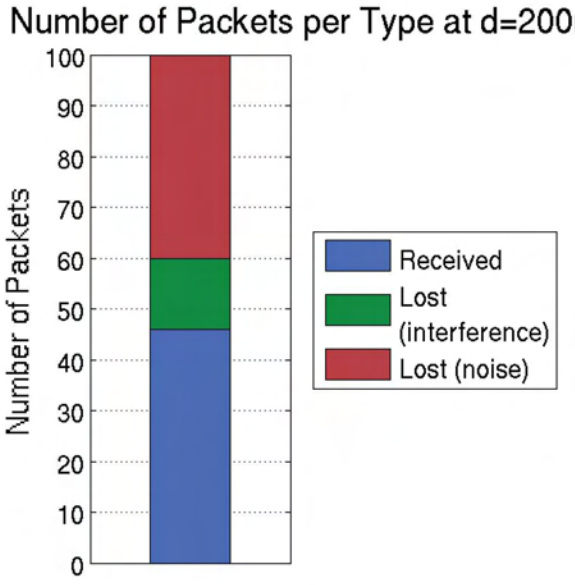

Figure 27: Bar plot for one 250B packet case

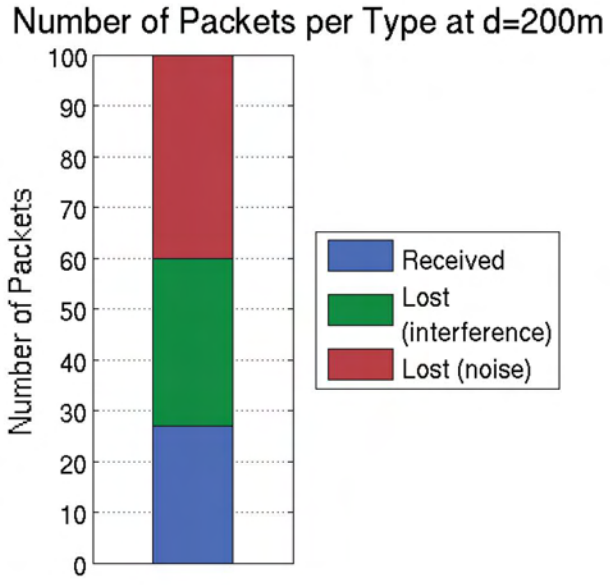

Figure 28: Bar plot for five 50B packets case

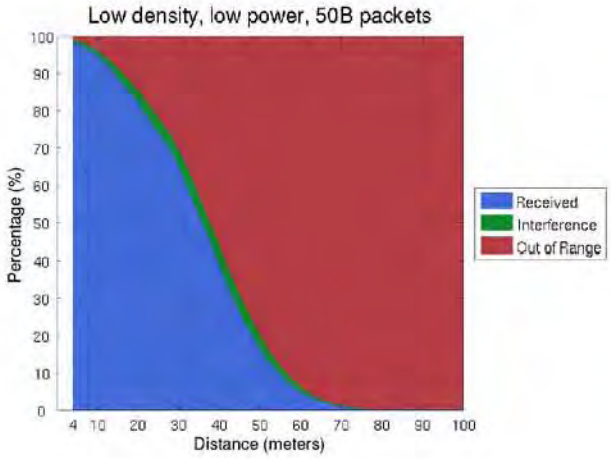

Figure 29: d=30m, P_{tx}=0dBm, 5x50B packets

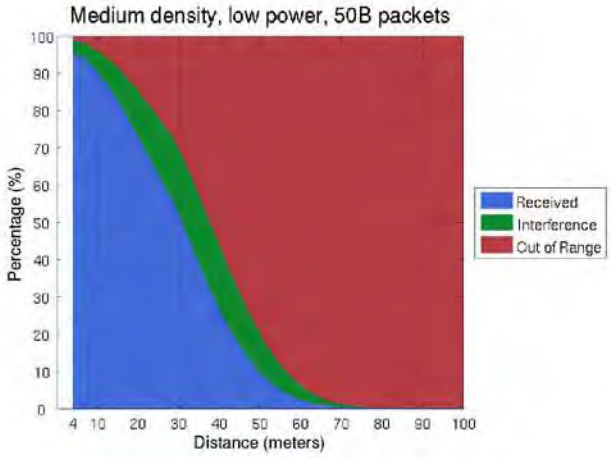

Figure 30: d=10m, P_{tx}=0dBm, 5x50B packets

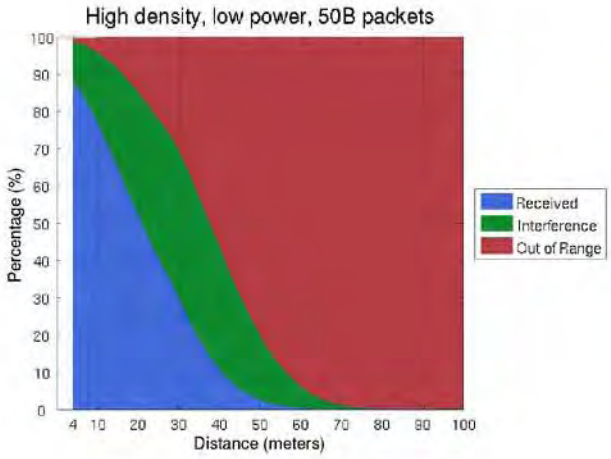

Figure 31: d=5m, P_{tx}=0dBm, 5x50B packets

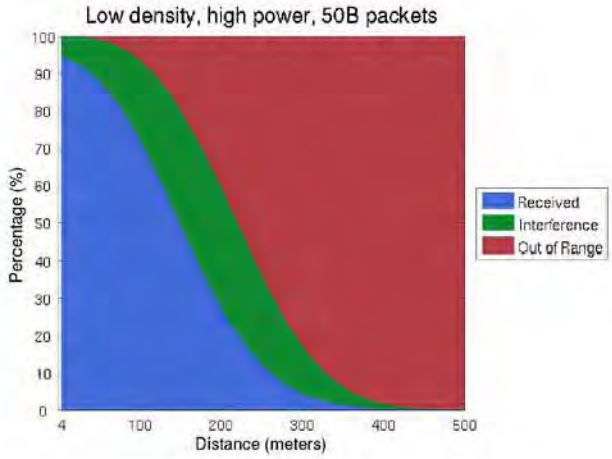

Figure 32: d=30m, P_{tx}=23dBm, 5x50B packets

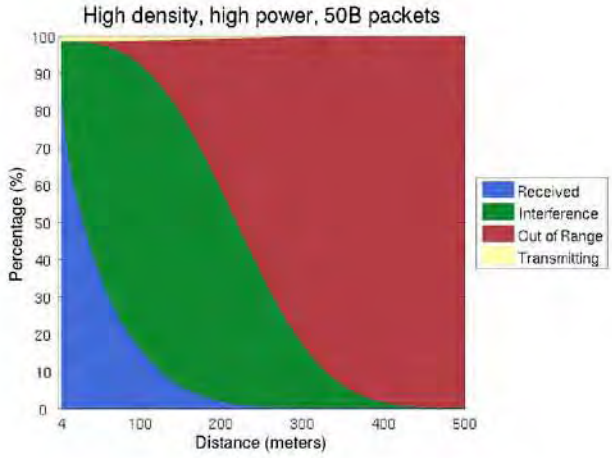

Figure 33: d=10m, P_{tx}=23dBm, 5x50B packets

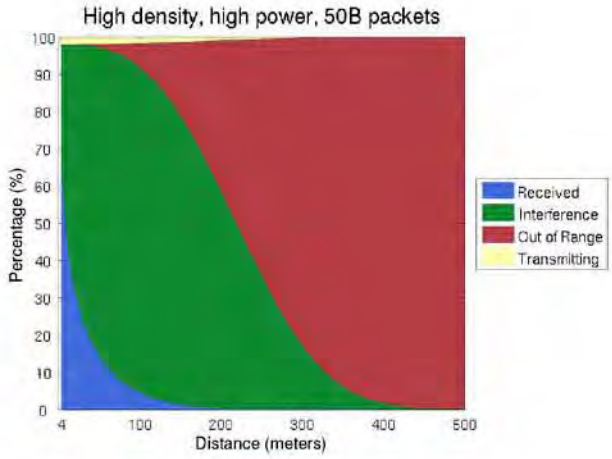

Figure 34: d=5m, P_{tx}=23dBm, 5x50B packets

3. Probability of Reception for Short-Range scenario

For short range communication, the Rayleigh fading model may not be appropriate. As mentioned before, this model is widely used for situations where a line-of-sight signal is not present, and there are many multipath signals. In the short-range scenario, one could expect that a line-of-sight scenarion is present. In this case, a Rician fading model can be used. In the actual implementation, we approximated a Rician channel by using a three-segment Nakagami channel with the following parameters:

$$\omega = \begin{cases} 2.0 & 0 < d < 30m \\ 3.0 & d > 30m \end{cases} \qquad \mu = \begin{cases} 1.5 & 0 < d < 70m \\ 1.0 & 70 < d < 110m \\ 0.75 & d > 110m \end{cases}$$

Below are the simulation results for a short-range communication scenario. Nodes transmitted 250B packets at 10Hz, just like before. The difference is that in these simulations a Nakagami fading model was utilized instead of a Rayleigh fading model.

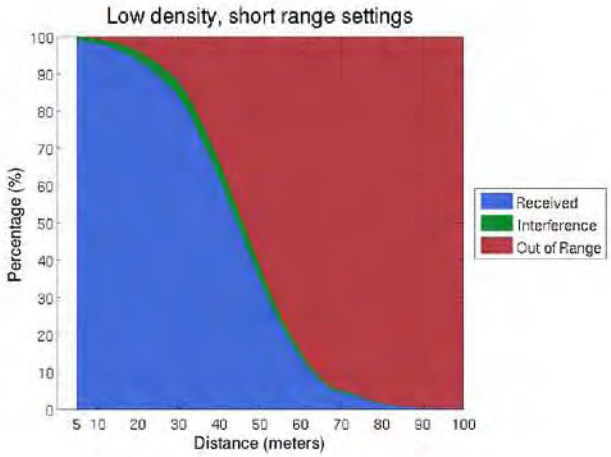

Figure 35: d=30m, P_{tx}=0dBm, single 250B packet, Nakagami fading (compare with Figure 16)

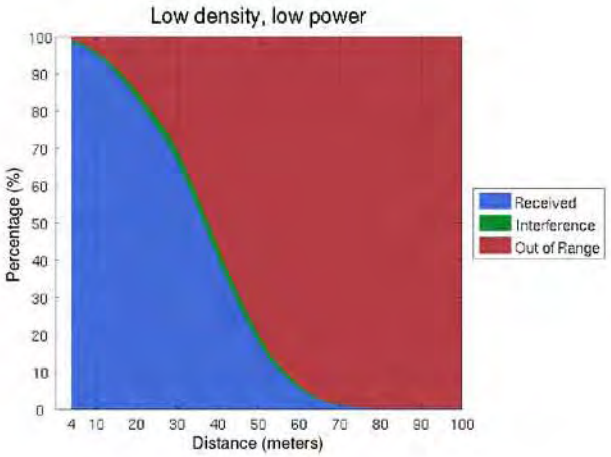

Figure 37: d=30m, P_{tx}=0dBm, single 250B packet

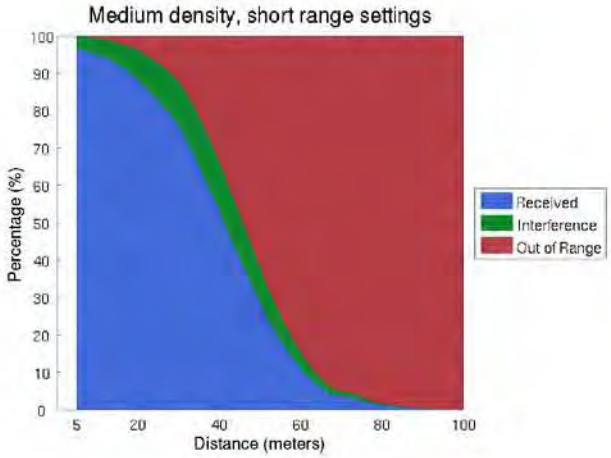

Figure 36: d=10m, Ptx=0dBm, single 250B packet, Nakagami fading (compare with Figure 18)

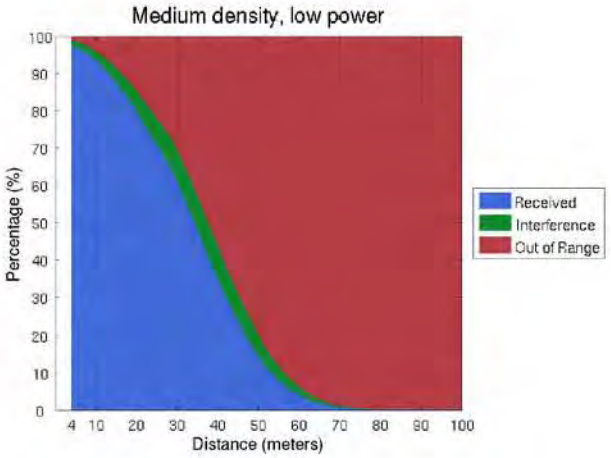

Figure 38: d=10m, P_{tx}=0dBm, single 250B packet

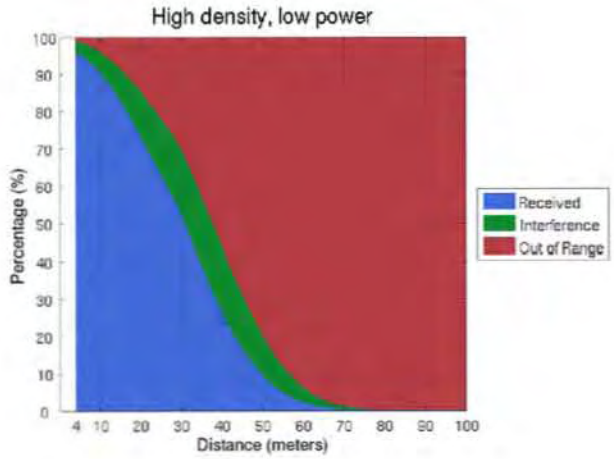

Figure 39: d=5m, Ptx=0dBm, single 250B packet, Nakagami fading (compare with Figure 20)

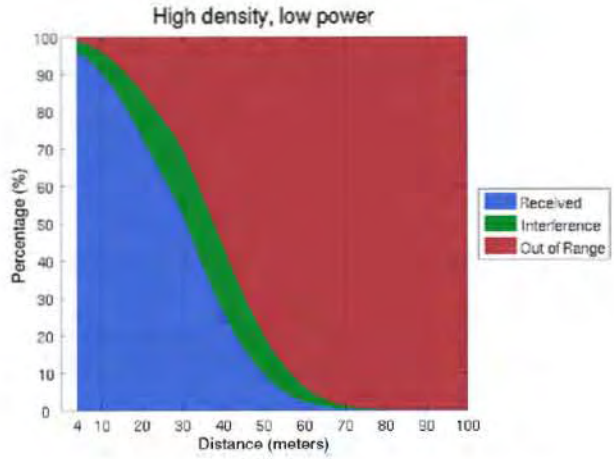

Figure 40: d=5m, Ptx=0dBm, single 250B packet

The results show that there's increased interference overall with Nakagami fading. This is most likely due to the fact that nearby nodes' line-of-sight signal is interfering with the received signal. However, note that even with increased interference, the 90% packet reception range is greater than the Rayleigh fading case. This is due to the line-of-sight component of the received signal. For low density, the range increases from 15m to 25m; for medium density from 12m to 18m; and for high density from 10m to XXm.

D. Conclusion

We have constructed NS-2 simulations of vehicular networks utilizing the 802.11Ext extension module. In the background section, we discussed how transmit power, pathloss, fading, and interference affect the probability of reception. We decided to use a Rayleigh fading model for the channel and to plot Probability of Reception vs. Distance curves to access system performance. These curves are helpful in determining achievable range given a specific reliability requirement, or vice-versa.

In our simulations, we varied the separation distance between transmitter and receiver and confirmed that interference increases as vehicle density rises. We found that utilizing a high transmit power (23dBm) was beneficial in the low and medium vehicle density (30m and 10m) scenarios because of larger range compared to low power (0 dBm). However, for the high density case (5m) low power has better performance because of there's too much interference with high transmit power. Furthermore, we determined that smaller packet sizes are detrimental to system performance because of the additional overhead needed in sending a greater number of messages, which is required to keep the data rate equivalent. We also found that 90% reception range is increased in short-range scenarios when using a Nakagami fading model versus a Rayleigh model.

The code produced through this work can be utilized for testing other system parameters and their effect on packet reception and range. An extension for this work would be to explore latency in addition to range and reliability, which is of great importance in safety applications.

E. References

[1] Qi Chen, Felix Schmidt-Eisenlohr, Daniel Jiang, Marc Torrent-Moreno, Luca Delgrossi, and Hannes Hartenstein. 2007. Overhaul of IEEE 802.11 modeling and simulation in ns-2. In Proceedings of the 10th ACM Symposium on Modeling, analysis, and simulation of wireless and mobile systems (MSWiM '07). ACM, New York, NY, USA, 159-168.

[2] "The Network Simulator - ns-2." [Online] Available: http://www.isi.edu/nsnam/ns/.

[3] Couch, Leon W. "Digital and Analog Communication Systems." Prentice Hall, 2007.

[4] Rappaport, Theodore S. "Wireless Communications: Principles and Practice." Prentice Hall PTR, 2002.

[4] "Noncentral chi-square distribution." Wikipedia, Feb. 2011 [Online] Available: http://en.wikipedia.org/wiki/Noncentral_chi-square_distribution

[5] "Fundamentals of Wireless Communication." Center for Wireless Technologies Eindhoven, [Online] Available: http://www.wirelesscommunication.nl/reference/contents.htm

[6] Richards, Mark. “Rice Distribution for RCS.” Feb. 8, 2010 [Online] Available: http://users.ece.gatech.edu/mrichard/Rice%20power%20pdf.pdf

[7] Jijun Yin; Holland, G.; ElBatt, T.; Fan Bai; Krishnan, H.; , "DSRC Channel Fading Analysis from Empirical Measurement," Communications and Networking in China, 2006. ChinaCom '06. First International Conference on, vol., no., pp.1-5, 25-27 Oct. 2006.

[8] “Nakagami distribution.” Wikipedia, Feb. 2011 [Online] Available: http://en.wikipedia.org/wiki/Nakagami_distribution

IV. Interference Analysis for 802.11p

A. Introduction

The goal of this work is to investigate the effect of interference on the performance of vehicular communication networks. The 802.11p standard assigns 7 adjacent 10 MHz channels for DSRC. Interference is caused when multiple radios, within a relatively small radius from one another, try to communicate at the same time. This is akin to a scenario where a group of people sharing a small room are trying to hold a number of side conversations simultaneously. The resulting noise will prevent the people from recognizing the messages directed to them. There are two kinds of interference in wireless communication networks: co-channel and adjacent channel interference. In this study, we focus here on adjacent channel interference.

In adjacent channel interference, the interferer is operating on a channel that is adjacent to the channel on which the considered transmitter-receiver pair is operating. Due to hardware non-idealities, part of the interferer's frequency spectrum spills onto its adjacent channel causing the interferer to behave as if it is operating on the same channel as the considered transmitter-receiver pair. Interference causes an increase in the effective noise level and, hence, an increase in the message error rate. Accordingly, the allowed level of interference is regulated by the IEEE where the output spectrum of all radios should fit within a spectral mask. The mask suppresses the out-of-band part of the interferers' signal. The masks imposed by the IEEE 802.11p standard (D5.0), for four different device classes, scaled by the interferers' transmission power are shown in Fig. 41. The masks suppress the spilled interference noise by -23.4 dB, -24.7 dB, -36.3 dB and

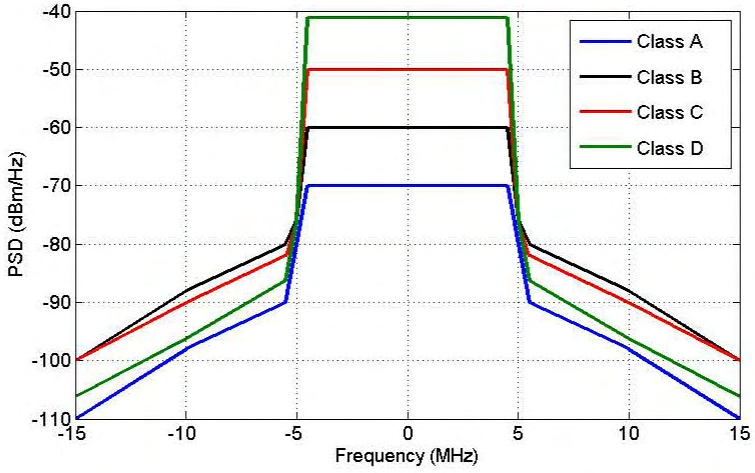

Figure 41: IEEE 802.11p Spectral Masks

-48.7 dB for classes A, B, C and D, respectively. The effect of interference, however, is amplified by the near-far problem. To understand this problem, revisiting the scenario where a group of people are talking to one another in a small room, imagine if the person you are trying to listen to is at the other side of the room, while there is a person standing right next to you that is talking.

As the rate of decay of sound waves is approximately proportional to the square of the traveled distance, the noise caused by the nearby speaker will make it much harder to recognize what the distant person is saying. Regarding wireless communications, the received single power can be approximated according to the simplified path loss model to

$$P_r = P_t\left(\frac{d_0}{d}\right)^{\gamma}\left(\frac{\lambda}{4\pi d_0}\right)^2,$$

where P_r is the received signal power, P_t is the transmitted signal power, d_0 is the reference distance for the antenna far-field, d is the distance between the transmitter and the receiver, γ is the path loss exponent and λ is the signal wavelength. The expression for the interference signal power at the receiver follows that of the received signal power with an added constant that accounts for the mask suppression. The noise power at the receiver radio can be expressed as

$$P_n = N_0 B F,$$

where P_n is the noise power, N_0 is the noise power spectral density, B is the operating bandwidth and F is the noise figure. The resulting signal to interference and noise ratio, *SINR*, can be expressed as

$$SINR = \frac{P_r}{P_i + P_n} = \frac{P_r/P_n}{1 + P_i/P_n} = \frac{SNR}{D},$$

where P_i is the interference signal power, *SNR* is the signal to noise ratio and D is the degradation in the effective *SNR* caused by interference. D can be expressed as

$$D\ (in\ dB) = 1 + \frac{KMP_{ti}{d_{0i}}^{\gamma_i - 2}}{{d_i}^{\gamma_i} F},$$

where M is the mask suppression, P_{ti} is the interferer's transmit power, d_{0i} is the reference distance for the antenna far-field for the interferer, γ_i is the interferer's path loss exponent, d_i is the distance between the interferer and the receiver, and K is defined as

$$K = \frac{1}{N_0 B}\left(\frac{\lambda}{4\pi}\right)^2.$$

As the distances between the transmitter and the receiver, *d,* and the interferer and the receiver, d_i, are random variables, the resulting *SNR* and D are both random variables as well. We derived expressions for the probability distribution functions (PDFs) of *d*, *di* and the resulting *SNR* and D. We used these expressions to calculate the resulting cumulative distribution functions (CDFs) of SNR and D. The CDF function is defined as the percentiles of the range of values of the random variable. We verified our results using simulations by Matlab and by a widely used wireless network simulator (NS2). We did our study for both the frequency plan proposed by 802.11p.

B. The 802.11p frequency plan

The frequency plan proposed by 802.11p is presented in Table 2. The table shows the 7 DSRC channels with their application, transmission power and the device class. The channels in this study are assumed to be reused every 1 kilometer, that is, the roads are divided into clusters of length 1 Km where vehicles sharing the same cluster can communicate with one another over the 7 channels. The resulting PDF of the distance between the transmitter and the receiver is hence given by

$$p(d) = \frac{1}{500}\left(1 - \frac{d}{1000}\right), 0 \leq d \leq 1000\ meters$$

$$p(d) = 0, otherwise.$$

Table 2: 802.11p Frequency Plan

Channel Number	Type	Maximum Transmit Power (dBm)	Mask
172	Safety	33	D
174	Services	33	D
176	Services	33	D
178	Control	44.8	D
180	Services	23	C
182	Services	23	C
184	Safety (Intersections)	40	D

The PDF of d_i follows that for d for cases where the interferer is another vehicle and not a road side unit. Combining the PDF of d with the expressions for *SNR* and *SINR*, the PDFs of *SNR* and *SINR* were derived for all the 7 channels. The analysis was done assuming an Additive White Gaussian Channel (AWGN) with $\gamma = \gamma_i = 2$ and $\gamma = \gamma_i = 2.4$. The NS2 simulations were extended to cover communicating over a flat fading channel with $\gamma = \gamma_i = 2$. The expressions are omitted for the brevity of the report.

The analysis had to be done for all 7 channels due to the asymmetry in the frequency plan. First of all, the maximum transmit power level and the number of neighboring channels vary across the 7 channels. Moreover, regarding channel 178, not only mobile vehicles but also road side units (RSUs) are allowed to operate on the channel. This has a direct effect on the effective SINR. Considering channel 172, there is a proposition to make the vehicles have 2 radios, where one radio operates on the safety channel (channel 172), and the other radio operates on one of the other 7 channels. This implementation may results in very high interference levels if the vehicle communicates on channel 172 and its neighboring channel (Channel 174) on its 2 radios. Thus, the resulting *SNR* and *SINR* CDFs are investigated for 2 scenarios: one representing a worst case scenario in which the transmitter communicates on channels 172 and 174 all the time and one in

which the transmitter communicates on both channels for a fraction of time that is equivalent to ratio between the vehicle's traffic and the overall network traffic on these channels.

The following assumptions were made for our study:

1. The analytical work assumes only 1 interferer per channel.
2. The analytical work assumes channel utilization of 100% by the interferer thus it serves as an upper bound on the CDFs of the *SINR* (for 1 interferer per channel).
3. The transmitted signals saturate the transmitters' masks.
4. Non-adjacent channel interference is neglected. For example, the interferer caused by channel 176 on channel 172 is neglected.
5. The simplified path loss model with $d_0 = 1$ is assumed.

Results showing the CDFs of *SNR* and *SINR* for the 7 channels are shown in Fig. 42. Results show that the analytical expressions, in most cases, serve as an upper bound on the degradation in performance caused by adjacent channel interference. However, this is not the case for the "double utilization" simulation scenarios where the network traffic of the interferer's channel is assumed to be twice the channel's capacity. Yet, this scenario is not supposed to happen as it would cause a huge deterioration of performance in the interferer's channel. It is presented in this work to test the performance of the system in "further than worst case" scenarios. A summary of the interesting observations regarding Fig. 42 is presented in Table 3.

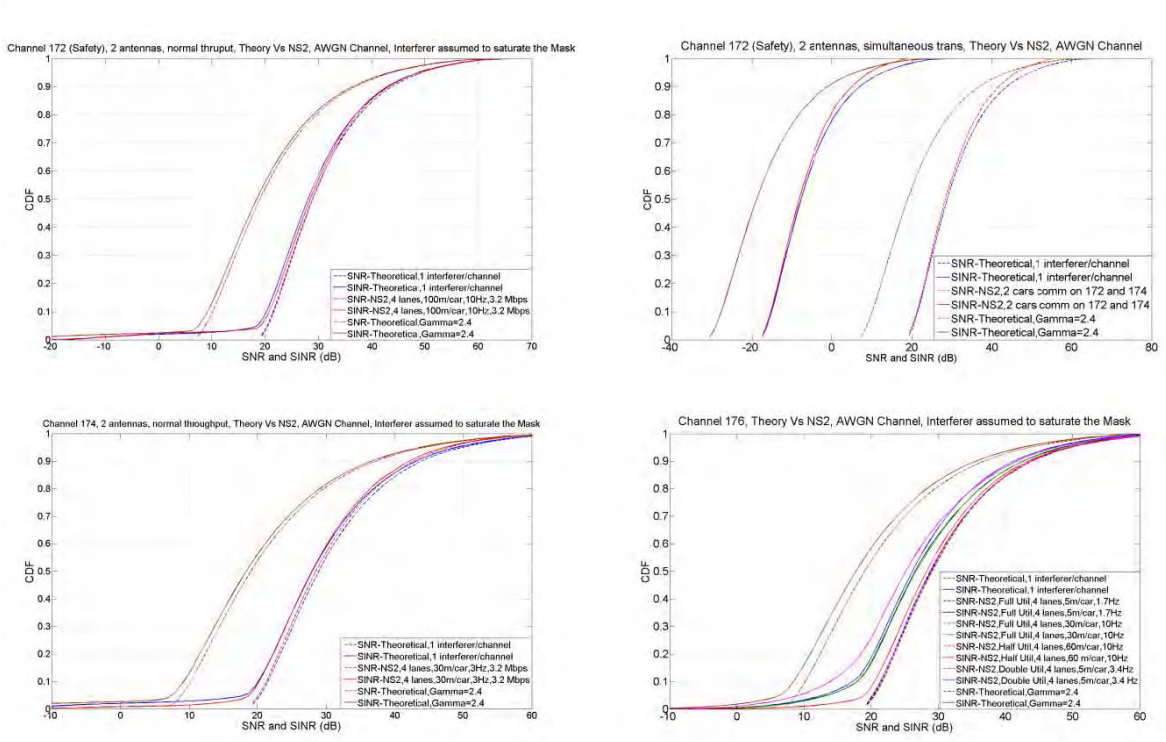

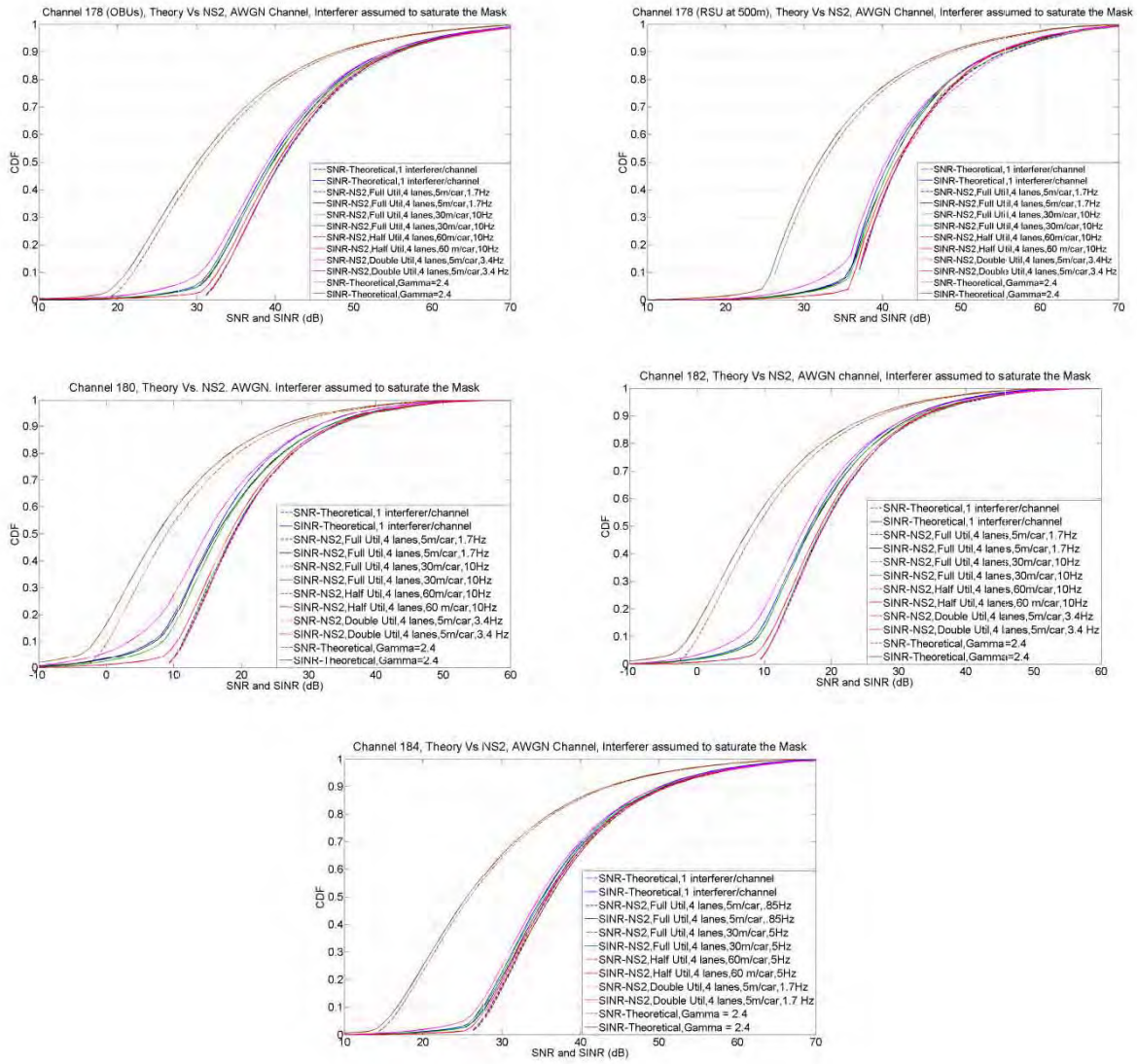

Figure 42: CDFs for SNR and SINR

Results show that over 90% of the time, the degradation in *SNR*, *D*, caused by adjacent channel interference is below 5 dB and 2 dB for $\gamma = 2$ and $\gamma = 2.4$ for an AWGN channel, respectively. Besides, the upper bound on degradation is the same for the flat fading channel case. However, regarding channel 172, if the vehicle has 2 separate radios that transmit simultaneously on channels 172 and 174, the resulting degradation in SNR is as high as 36 dB. This means that the effective power that the receiver "sees" is decreased by a factor of about 4000 because of the adjacent channel interference. The 10^{th} percentile effective *SINR* for the 7 channels ranges between 7 dB to 35 dB for an AWGN channel with $\gamma = 2$. Yet, for channel 172, the 10^{th} percentile effective *SINR* is -15 dB which is too low for conventional modulation techniques.

Table 3: Effective SINR under different channel models

Channel Number	AWGN, $\gamma = 2$		AWGN, $\gamma = 2.4$		Flat Fading, $\gamma = 2$	
	10^{th} Percentile *SINR* (dB)	10^{th} Percentile *D* (dB)	10^{th} Percentile *SINR* (dB)	10^{th} Percentile *D* (dB)	10^{th} Percentile *SINR* (dB)	10^{th} Percentile *D* (dB)
172 (Normal Throughput*)	20	2	8	2	-	-
172 (Sim Comm.**)	-15	36	-28	38	-	-
174	20	2	8	2	15	1.5
176	17	5	8	2	12	4.5
178 (OBUs)	32	2	21	1	-	-
178 (RSU-OBU)	35	2	25	1	-	-
180	7	5	-2	2	1	5
182	8	4	-2	2	2.5	3.5
184	27.5	1.5	16.5	1	22.5	1

*Every car has 2 antennas that are 0.5 m apart, one operating at channel 172, the other at channel 174. The network traffic is divided upon 45 vehicles.

** Every car has 2 antennas that are 0.5 m apart, one operating at channel 172, the other at channel 174. Communication between only 2 vehicle is considered that are communicating on both channels simultaneously.

C. Conclusion

In this study, we analyze the effect of adjacent channel interference on the performance of DSRC networks. We verified our analysis with NS2 simulations. Results show that, for the 802.11p frequency plan, the resulting 10^{th} percentile effective SINR is in a range that is suitable for the conventional modulation techniques. However, this is not the case for the safety channel if the vehicles are equipped with 2 radios that simultaneously transmit on the safety channel and its neighboring channel. This issue has to be addressed where interference can be decreased, for example, by avoiding or decreasing the probability of the simultaneous communication on both channels.

V. Localization

A. Introduction

One of the key assumptions in most accident avoidance algorithms is the ability to locate the vehicles within a small margin of error. The error margin in some applications is as low as 0.5 meters. Besides, knowledge of the vehicles' velocity, acceleration and other data related to the vehicle dynamics is recommended. When the information about the positions of the vehicles and their trajectories is shared, various safety algorithms can be applied to predict and avoid accidents.

We present two different approaches for accurate localization of vehicles. The first approach relies on estimating the relative distances between vehicles by analyzing the strength of the communication signals between them. The second approach relies on Global Positioning System (GPS) data.

B. Received Signal Strength (RSS) based localization

Wireless communication signals attenuate as they propagate. As the distance traveled by the signal increases, the signal becomes weaker. The relationship between the signal attenuation and the traveled distance has been an active subject of research. The distance between two points can thus be approximated within a margin of error provided that the strength of the signal at the starting and ending points is known.

One drawback of RSS is that it c an be used in estimating the relative position between vehicles rather than the absolute position of the vehicles. However, in accident avoidance, the relative distance between the vehicles is sometimes enough to predict an accident. Besides, the RSS based localization algorithm can be combined with other localization mechanisms to estimate the absolute position of vehicles. For example, knowledge of the absolute position of one of the vehicles in a cluster through GPS is sufficient for estimating the absolute positions of all vehicles ion the cluster. This is of course provided that information about the relative positions of the vehicles is available.

Another drawback of RSS based localization is that the error in the estimated relative positions of the vehicles passes the maximum boundary of 0.5 meters. Accordingly, in this work, we test an algorithm proposed by [1] that improves the RSS based location estimates assuming the knowledge of an initial GPS-based location estimate. The model assumes the knowledge of an estimate of the vehicles' velocities. Using the initial position data, together with the continuous updates of the vehicles' velocities and the RSS data, the location of the vehicles can be estimated by applying a simple vehicle dynamics model. Besides, the proposed algorithm features the collaboration between all vehicles in the cluster to estimate their positions. The algorithm is presented in Fig. 43.

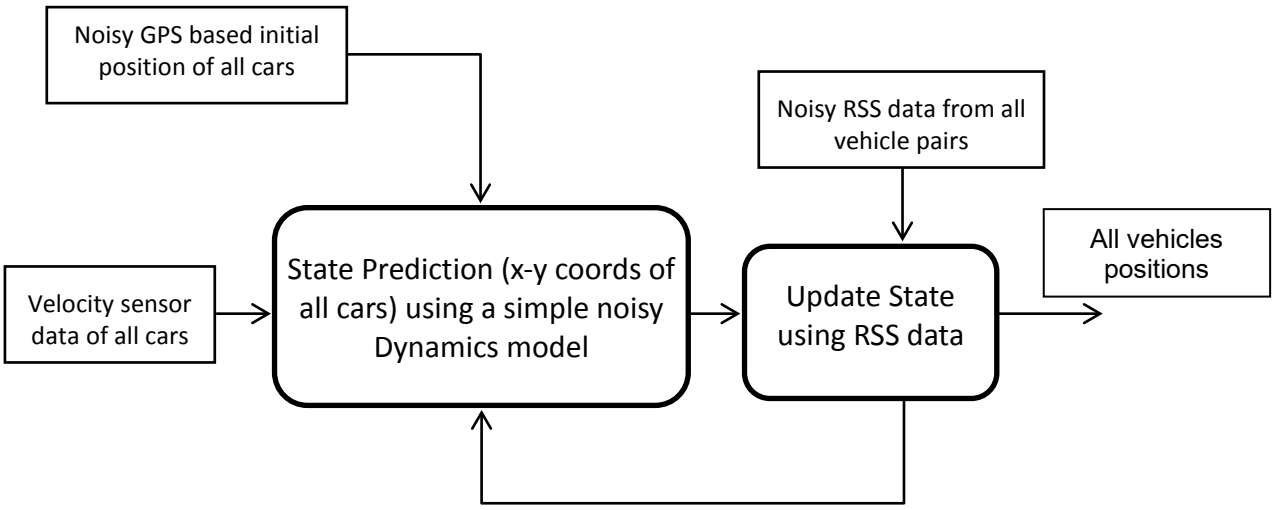

Figure 43: The tested RSS based Algorithm

We conducted the following tests on the model:

1. Impact of initial GPS estimate and RSS ranging error

In this test, we assume that a road boundary map is available. We test the effect of the error in the RSS data and the error in the initial GPS data on the error in the estimated relative positions of the vehicles. The results are shown in Fig. 44. The standard deviation of the initial GPS data is varied from 0.5 to 6 meters and the standard deviation of the error in the estimated

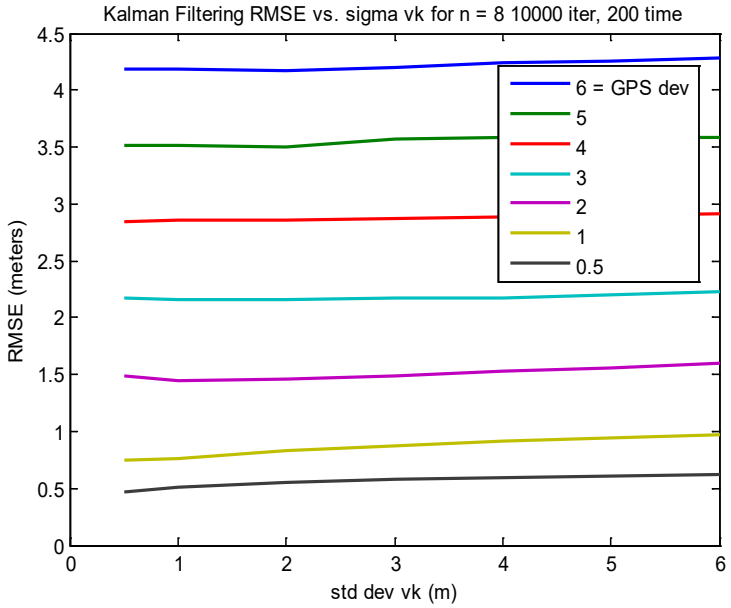

Figure 44: Impact of initial GPS estimate and RSS ranging error

distances between vehicle pairs (obtained from the RSS data) is varied from 0.5 to 6 meters. Results show that the error in the estimated vehicle positions after applying the algorithm depends mostly on the error in the intial GPS data. Besides, the error in the estimated locations can reach the 0.5 meters contraint imposed by the safety algorithms if the error in the intial GPS data has a standard deviation of less than 0.5 meters.

2. The effect of Road Boundary information and Collaboration

In this section we test the effect of adding the road boundary map data on the error in the estimated vehicle positions. We also investigate the effect of collaboration between vehicles on the performance of the localization algorithm. Results are shown in Fig. 45. The number of vehicles is increased from 3 to 20 vehicles. It is clear that increasing the number of collaborating vehicles decreases the error in position estimation. However, as the number of vehicles increases, the decrease in position error decreases. Moreover, results also show that adding the road

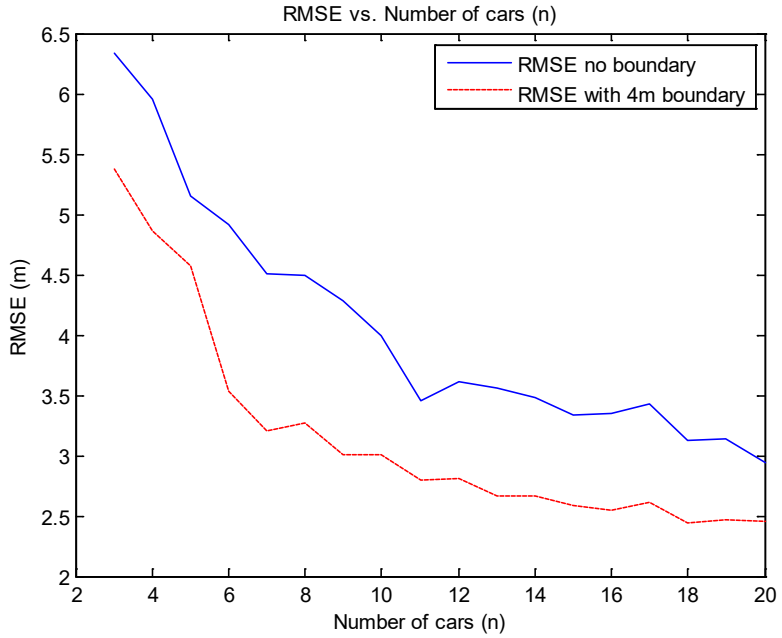

Figure 45: The effect of Road Boundary information and Collaboration

boundary information causes a decrease in the location estimation error by about 1 meter. For the tested scenario, for 20 vehicles, with round boundary information, the location estimation error reaches 2-2.5 meters asymptotically.

3. Incorporating vehicles with accurate initial position estimates

In this final test, we investigate the effect of having vehicles with an accurate initial GPS location data. The error in their initial GPS location data is assumed to have a standard deviation of 0.5 meters. The number of these vehicles is increased from 0 to 8 vehicles. The results are

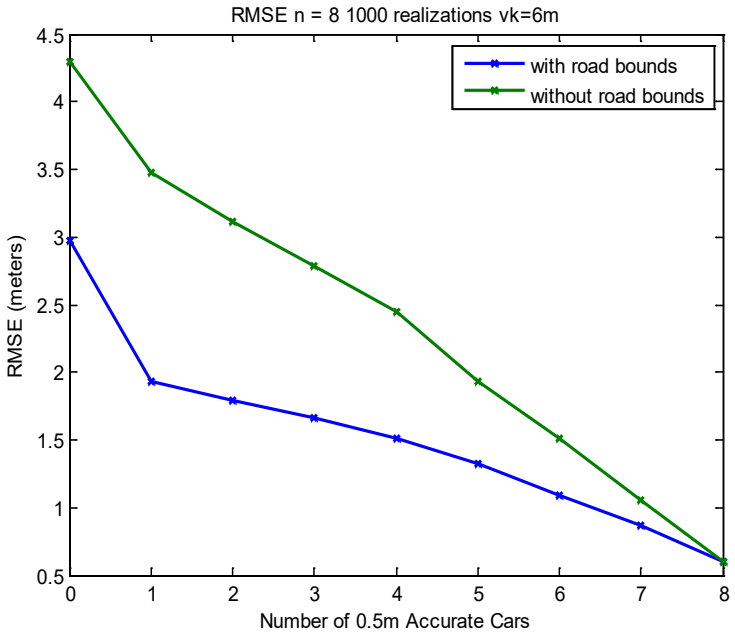

Figure 46: Incorporating vehicles with accurate initial position estimates

presented in Fig. 46. Results show that increasing the number of vehicles with accurate initial GPS data decreases the error in the estimated vehicles' positions. Besides, the results reaffirm the fact that adding road boundaries decreases the error.

4. Conclusions regarding testing the proposed RSS based localization algorithm

Our tests show that in order to achieve highly accurate localization based on RSS, collaboration between vehicles is needed. Besides, increasing the number of collaborating vehicles more than 15 vehicles does not show a significant improvement in performance. Furthermore, if the collaborating vehicles include vehicles that have highly accurate initial position information, the position estimation error for all vehicles can be reduced considerably. Moreover, adding the road boundary information to the model results in a decrease in the position estimation error that reaches as high as 1.5 meters.

5. Analyzing the effect of the uncertainty of the path loss exponent on RSS-based localization

In this section we study the effect of the error in the path loss exponent on the error in the estimated position. As mentioned earlier, RSS-based localization is based on estimating the distance traveled by wireless communication signals. The estimate has a high dependence on the path loss model. A commonly used path loss model is given as

$$P_r = P_t\left(\frac{d_0}{d}\right)^{\gamma}\left(\frac{\lambda}{4\pi d_0}\right)^2$$

Where the variables are as defined in Section 1. As the path loss exponent, γ, is considered random, there are algorithms designed to estimate it. However, γ can only be estimated with a margin of error. We denote the error in γ by ε. The error in the estimated distance, $\tilde{d}$, as a function of ε is defined as

$$\tilde{d} = d - d^{\frac{\gamma}{\gamma+\varepsilon}}$$

ε is assumed to have a normal distribution with an average of 0 and a variance of $\sigma_\varepsilon{}^2$. Define the normalized position error as

$$\bar{d} = \frac{\tilde{d}}{d},$$

then the PDF of $\bar{d}$ can be expressed as

$$p(\bar{d}) = \frac{\gamma log(d) e^{\frac{-\gamma^2}{2\sigma_\varepsilon{}^2}\left[\frac{log(1-\bar{d})}{log(d(1-\bar{d}))}\right]^2}}{\sqrt{2\pi}\sigma_\varepsilon(1-\bar{d})\left[log\left(d(1-\bar{d})\right)\right]^2}.$$

The second moment of $\bar{d}$ can thus be derived as

$$E\{\bar{d}^2\} = \sum_{n=1}^{\infty}\frac{\log(d)^n}{n!}\sum_{m=0}^{\infty}\binom{m+n-1}{m}\frac{(-1)^{m+n}}{\gamma^{m+n}}\sum_{p=1}^{\infty}\frac{\log(d)^p}{p!}\sum_{q=0}^{\infty}\binom{p+q-1}{q}\frac{(-1)^{p+q}}{\gamma^{p+q}}E\{\varepsilon^{m+n+p+q}\},$$

where

$E\{\varepsilon^x\} = 0$ for odd x and $[\sigma_\varepsilon{}^x x!!]$ for even x.

Fig. 47 shows the variation of the standard deviation of the normalized position error with distance. Results are shown for three values of σ_ε, 0.1, 0.15 a nd 0.2. Results show that the accuracy of the RSS based localization algorithm has high sensitivity towards the error in the path loss exponent and the distance between the transmitter and receiver of the localization signal. For instance, the standard deviation of the location error is about 45 meters for $\sigma_\varepsilon = 0.5$ where the distance between the transmitter and the receiver is 100 meters.

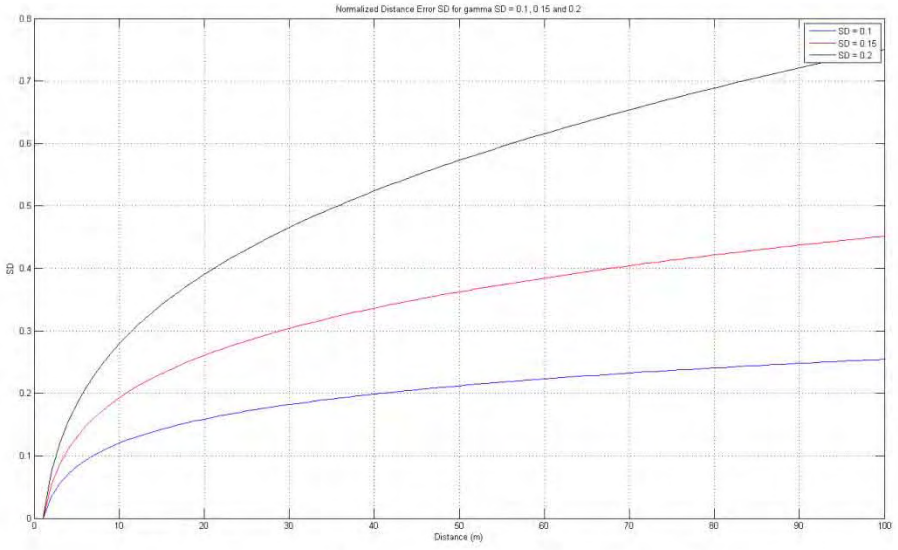

Figure 47: Standard Deviation of the Normalized distance error

C. GPS based localization

The GPS system is made of 30 Satellites rotating in 6 orbits. The satellites send message beacons containing information about their orbit information with time stamps. GPS receivers use the data to estimate their positions. For location estimation, there are 4 unknowns, the 3 spatial coordinates of the GPS receiver and time synchronization information between the receiver's clock and the GPS' system clock. Hence, at least 4 satellites are needed to obtain an estimate for the location.

The main sources of error for GPS localization include Ionospheric and Tropospheric propagation errors (which mostly cause a bias error), multipath errors (which result in bias as well as random errors), Ephemeris data errors (errors in the satellite orbital information), satellite clock errors and receiver errors.

A literature survey was carried out in order to investigate whether GPS based localization can result in an acceptable localization error. According to [2], [3] and [4], GPS data can be combined with vehicle sensor data using a Kalman filter that is based on a vehicular dynamics model. This combination results in an error in the 20-30 cm range under acceptable GPS coverage, about 50 cm of error with occasional GPS outage and multipath errors caused by trees and buildings and up to 1 meter with long GPS outages and big changes in the vehicle's trajectory. Thus, GPS localization, in most scenarios, can results in an acceptable localization error that is below 50 cm.

D. Conclusion

There are 2 different mechanisms for localization explored in this work. RSS based localization is cheaper to implement as it does not require extra hardware. However, the localization error using RSS often passes the maximum limit recommended by safety

applications. The error in RSS based localization can be reduced by allowing the collaboration between vehicles for localization, providing information about the road boundary information and incorporating the vehicle's dynamics model. On the other hand, GPS based localization can, in most scenarios, result in an acceptable localization error. Yet, GPS based localization requires extra hardware for receiving the GPS signals.

E. References

[1] R. Parker and S. Valaee, "Vehicular node localization using received-signal-strength indicator," *IEEE Transactions on Vehicular Technology*, vol. 56, no. 6, part 1, pp. 3371-3380, 2007.

[2] Skog, I.; Handel, P., "In-Car Positioning and Navigation Technologies—A Survey," Intelligent Transportation Systems, IEEE Transactions on, vol.10, no.1, pp.4-21, March 2009.

[3] Jihua Huang; Tan, H.-S., "A Low-Order DGPS-Based Vehicle Positioning System Under Urban Environment," Mechatronics, IEEE/ASME Transactions on , vol .11, no.5, pp.567 -575, Oct. 2006.

[4] Rezaei, S.; Sengupta, R., "Kalman Filter-Based Integration of DGPS and Vehicle Sensors for Localization," Control Systems Technology, IEEE Transactions on , vol.15, no.6, pp.1080-1088, Nov. 2007.